Recovery of the first ever multi-year lidar dataset of the stratospheric aerosol layer, from Lexington, MA, and Fairbanks, AK, January 1964 to July 1965.

Juan-Carlos Antuña-Marrero[1], Graham W. Mann[2,3], John Barnes[4], ~~Albeth~~Albeht Rodríguez-Vega[5], Sarah Shallcross[2], Sandip S. Dhomse[2,~~3~~4], Giorgio Fiocco[†] and Gerald W. Grams[†]

[1]~~Departamento de Física Teórica, Atómica y Óptica,~~[1]Group of Atmospheric Optics (GOA-UVa), Universidad de Valladolid, ~~4700~~47011, Valladolid, Spain

[2]School of Earth and Environment, University of Leeds, Leeds, LS2 9JT, UK.

[3]National Centre for Atmospheric Science (NCAS-Climate), University of Leeds, Leeds, UK

[4]~~NOAA~~[4]National Centre for Earth Observation (NCEO), University of Leeds, Leeds, UK

[5]NOAA, ESRL Global Monitoring ~~Division~~Laboratory, Colorado, US

[5]~~Grupo~~[6]Grupo de Óptica Atmosférica de Camagüey, Centro Meteorológico de Camagüey, INSMET, Cuba

[†]Deceased

Correspondence to: Juan-Carlos Antuña-Marrero (antuna@goa.uva.es)

Abstract. We report the recovery and processing methodology of the first ever multi-year lidar dataset of the stratospheric aerosol layer. A Q-switched Ruby lidar measured 66 vertical profiles of 694nm attenuated backscatter at Lexington, Massachusetts between January 1964 and August 1965, with an additional 9 profile measurements conducted from College, Alaska during July and August 1964. We describe the processing of the recovered lidar backscattering ratio profiles to produce mid-visible (532nm) stratospheric aerosol extinction profiles ($sAEP_{532}$) and stratospheric aerosol optical depth ($sAOD_{532}$) measurements, utilizing a number of contemporary measurements of several different atmospheric variables. Stratospheric soundings of temperature, and pressure generate an accurate local molecular backscattering profile, with nearby ozone soundings determining the ozone absorption, ~~those profiles then~~which are used to correct for two-way ozone transmittance. Two-way aerosol transmittance corrections ~~were~~are also applied based on nearby observations of total aerosol optical depth (across the troposphere and stratosphere) from sun photometer measurements. We show ~~the~~ that accounting for these two-way transmittance ~~correction has substantial~~ effects ~~on the retrieved $sAEP_{532}$ and $sAOD_{532}$, calculated without the corrections resulting in~~ substantially ~~lower values of both variables, as it was not applied~~increases the magnitude of the 1964/5 stratospheric aerosol layer's optical thickness in the Northern Hemisphere mid-latitudes, then ~50% larger than represented in the ~~original processing producing~~ CMIP6 volcanic forcing dataset. Compared to the ~~lidar scattering ratio profiles we rescued. The~~ uncorrected dataset, the combined transmittance ~~corrections causes the aerosol extinction to increase~~correction increases the $sAOD_{532}$ by ~~67~~up to 66 % for Lexington and up to 27 % for Fairbanks, ~~for $sAOD_{532}$ the increases 66 % and 26 % respectively. Comparing the magnitudes~~individual $sAEP_{532}$ adjustments of ~~the aerosol extinction and sAOD~~similar magnitude. Comparisons with the few contemporary available measurements ~~reported~~ show ~~a~~ better agreement ~~in the case of~~with the two-way transmittance corrected values.

~~The sAEP and sAOD timeseries at Lexington show a surprisingly large degree of variability, three periods where~~Within the ~~stratospheric aerosol layer had suddenly elevated optical thickness, the highest $sAOD_{532}$ of 0.07 measured at the end of March 1965. The two other periods of enhanced $sAOD_{532}$ are both two-month periods where the lidars show more than 1 night~~

Definición de estilo: Normal
Definición de estilo: Texto comentario: Fuente: 11 pto
Definición de estilo: Default
Definición de estilo: Revisión
Con formato: Inicio de sección: Nueva página
Con formato: Inglés (Estados Unidos)
Con formato: Inglés (Estados Unidos)
Con formato: Inglés (Estados Unidos)
Con formato: Inglés (Estados Unidos)
Con formato: Inglés (Estados Unidos)
Con formato: Inglés (Estados Unidos)
Con formato: Sangría: Izquierda: 0 cm

where retrieved sAOD$_{532}$ exceeded 0.05: in January and February 1964 and November and to August 1965 measurement timespan, the corrected Lexington sAOD$_{532}$ timeseries is substantially above 0.05 in three distinct periods: October 1964, March 1965 and May-June 1965, whereas the 6 nights the lidar measured in December 1964. Interactive and January 1965 had sAOD at most ~0.03. Comparison with interactive stratospheric aerosol model simulations of the 1963 Agung aerosol cloud illustrateshows that, although substantial variation in mid-latitude sAOD$_{532}$ isare expected from the seasonal cycle in the Brewer-Dobson stratospheric circulation, the Agung cloudcloud's dispersion willfrom the tropics would have caused much slower increase than the more episodic variations observed, with also different timing, elevated optical thickness from Agung occurringbeen at its strongest in winter, and spring.weakest in summer. The abruptness and timing of the steadily increasing trend in sAOD from January to July 1965, also considering the large variability, suggests this variation wasthat the observed variations are from a different source than Agung, possibly from one or both of the two VEI3 eruptions that occurred in 1964/65: Trident, Alaska and Vestmannaeyjar, Heimey, south of Iceland. A detailed error analysis of the uncertainties in each of the variables involved in the processing chain was conducted, relative. Relative errors offor the uncorrected sAEP$_{532}$ were 54 % for Fairbanks and 44 % Lexington for. For the uncorrected sAEP$_{532}$, corrected sAEP$_{532}$ ofthe errors were 61 % and 64 % respectively. The analysis of the uncertainties, identified variables that, with additional data recovery and reprocessing could reduce these relative error levels. Data described in this work are available at *https://doi.pangaea.de/10.1594/PANGAEA.922105 (Dataset in Review)* (Antuña-Marrero et al., 2020a).

1. Introduction:

The abrupt enhancements to the stratospheric aerosol layer from historical large magnitude volcanic eruptions (e.g. Deshler, 2008) cause substantial radiative forcings toforcing of the Earth's climate system, and reducing. Reducing their uncertainty remains an important priority for international scientific research,since volcanic forcings beingcan be the strongest driver of natural climate variability (e.g. Hansen, 1978; Robock, 2000). One of the co-ordinatedcoordinated multi-model experiments within the current international ISA-MIP activity (Interactive Stratospheric Aerosol Model Intercomparison Project, Timmreck et al., 2018), involves simulations of the volcanic aerosol clouds from the largest volcanic eruptions in the last century, Mt. Agung in 1963, El Chichón in 1982 and Mt. Pinatubo in 1991. TheOne of the main motivation formotivations within this HErSEA multi-model experiment (Historical Eruption SO_2 Emission Assessment) is to gather stratospheric aerosol observations in the periods after major tropical eruptions to provide new contraints to evaluate the model simulations, and. Another is to seek to understand whether the current diversity in the sulphursulfur emission amount and altitude distribution interactivethat stratospheric aerosol models use when simulating the Pinatubo aerosol cloud is also seen for other major tropical eruptions such as Agung (see section 3.3.2 of Timmreck et al., 20082018). The first of the ISA-MIP modelling groups to present results from all three of the HErSEA eruption cloud experiments was recently published (Dhomse et al., 2020), with another). Another recent study focusingfocused on assessing the variability and global distribution of the Agung aerosol cloud (Niemeier et al., 2019).

Whereas the models participating in ISA-MIP simulate volcanic aerosol clouds interactively, the historical climate model simulations that provide the main basis for attributing past climate variability (Hegerl and Schwierz, 2011; Gillett et al., 2016)), use prescribed volcanic forcing datasets (e.g. Sato et al., 1993; Ammann et al., 2003; Luo, 2016; Thomason et al., 2018), reference aerosol optical properties used to enact volcanic surface cooling.). The observational data constraining the Agung aerosol cloud in both the interactive models and for the volcanic forcing datasets has hitherto tended to be based on column optical properties measured at the surface. These are primarily the extensive synthesis of surface radiation observations summarized by Dyer and Hicks (1968), with additional turbidity anomaly data from astronomical measurements of the atmospheric attenuation of starlight (Stothers, 2001). Although the literature includes several papers reporting profile measurements of the Agung aerosol cloud from balloon measurements (Rosen, 1964; 1968), lidars (Fiocco and Grams, 1964;

Clemesha et al., 1966) and searchlights (Elterman and Campbell, 1964), no profile dataset of Agung backscatter ratio or aerosol extinction has yet been available to the scientific community. Whereas the Jamaica lidar (Clemesha et al., 1966) also measured the Agung cloud, the first multi-year ~~dataset of~~ lidar measurements of the ~~volcanic aerosol from that~~Agung eruption ~~was~~were conducted from Lexington, Massachusetts from January 1964 to August 1965 (Grams and Fiocco, 1967, hereinafter **GF-67**). No digital record of these lidar measurements existed until now, the data apparently only presented in Figures ~~of the lidar backscattering ratio profiles~~ within published scientific papers~~, providing only~~. Only a few quantitative ~~information about the altitude of the Agung aerosol cloud. Although the descent in the peak of the backscatter ratio profile from Lexington is analysed within GF-67, only limited~~ estimates of the cloud's optical properties from the lidar dataset have been found; aerosol extinction ~~exist (~~of 2 x 10^{-3} km^{-1} at 16 km and the aerosol optical depth of 0.015 (Deirmejian, 1971~~) were been produced.~~).

~~We discovered however~~However, after initial ~~search~~failed searches of digital archives at several institutions, we discovered that the original lidar ~~backscattering~~backscatter ratio profile measurements from the Lexington and Alaska 1964/5 soundings are fully tabulated in Gerald W. Grams PhD thesis conducted under the supervision of Prof. ~~Giogio~~Giorgio Fiocco (Grams, 1966) hereinafter identified as **G-66**. Fortunately, at those times it was quite common for some observational datasets to be tabulated within PhD theses or grant reports etc., a practice that after several decades is becoming required again, with many journals now mandating authors to make available the data they use via a ~~recognised~~recognized open-access data archive.

Dhomse et al. (2020) used preliminarily processed lidar data from Lexington, MA, one of the two sites reported in (**GF-67**) to compare model aerosol extinction at 16 km with lidar observations, finding good agreement. ~~They~~Dhomse et al. (2020) and Niemeier et al. (2019) also noted the large ~~differences between~~ change in the ~~CMIP5 and CMIP6~~ volcanic ~~aerosol datasets~~forcing for the Agung ~~and El Chichón~~ periods, ~~pointing out~~with the volcanic aerosol datasets used in the Coupled Model Intercomparison Projects 5 and 6 (CMIP5, Taylor et al., 2012; and CMIP6, Eyring, et al., 2016; Zanchettin et al., 2016). The importance of reducing ~~this~~ uncertainty by reconciling the datasets with additional stratospheric aerosol observations~~. There only~~ was also identified within these studies. Only an initial (preliminary) ~~single-level~~ version of the Lexington 550nm aerosol extinction dataset was used~~, our~~ in Dhomse et al. (2020), with the analysis here ~~completing the processing of the full~~ producing a vertical profile ~~(~~dataset between 12 and 24km~~), with~~. An important aspect of the dataset here is the two-way transmittance corrections applied to the aerosol backscatter ratio, when deriving the aerosol extinction and optical depth datasets, with also ~~with~~ a detailed and transparent assessment of the relative error in each ~~metric~~quantity included.

This work is a contribution to the Data Rescue activity of the Stratospheric Sulfur and its Role in Climate (SSiRC) a SPARC initiative (SSiRC, 2020~~), following a recent~~). The 1964/65 lidar data recovered here follows on from another important volcanic aerosol dataset recovery, of two ship-borne lidar datasets that measured the progression of the highly uncertain "tropical core" of the Pinatubo aerosol cloud in July 17th to September 13th 1991, 4-12 weeks after the 15th June 1991 Pinatubo eruption (Antuña-Marrero et al., 2020b). Those datasets were an identified priority ~~for~~within the SSiRC data ~~recovery, being in is~~rescue activity, since they provide new constraints within the period when the Stratospheric Aerosols and Gas Experiment II (SAGE II) satellite could only observe the ~~stratospheric~~upper part of the Pinatubo aerosol ~~above around 22 km~~cloud, due to the ~~extreme opacity of the aerosols (~~saturation of the aerosol extinction retrieval (e.g. Thomason, 1992; McCormick and Veiga, 1992).

2. Materials and Methods.

2.1 Lidar instrumentation:

The first successful laser radar ranging experiment was conducted at the Research Laboratory of Electronics, Massachusetts Institute of Technology, at Lexington, Massachusetts, and consisted of ~~analysing~~analyzing the return signal from a ~~very high frequency (nano~~short pulse (micro-second) laser ~~and for~~covering the 60-140km altitude range (Smullin and Fiocco, 1962). The research team, led by Prof. Giorgio Fiocco, continued developing applications of the lidar for atmospheric research. Scattering layers were detected in the upper atmosphere between 110 and 140 km (Fiocco and Smullin, 1963) and were interpreted to originate from meteoric fragments entering the outer atmosphere (Fiocco and Colombo, 1964). After some changes and improvements, stratospheric aerosols were detected between 10 and 30 km altitude and the first lidar measurements of the stratospheric aerosol layer began (Fiocco and Grams, 1964).

The schematic diagram and a photo of the instrument are in figures 3 and 4 of **G-66** respectively. ~~There are~~Also listed ~~also~~are the main features of the ~~lidar instruments~~lidars used for the measurements at Lexington and College, Alaska, ~~reported in its table 1,~~ reproduced ~~below~~in Table 1. Both ~~instruments~~lidars used a Q-switched ruby laser, at the 694 nm wavelength.

~~Observation~~Observation period	January-May	July-August	~~October~~October 1964
~~Observation~~Observation site	Lexington	College	Lexington
Transmitted wavelength	0.694 µm	0.694 µm	0.694 µm
Pulse length	< 1 µs	< 1 µs	< 1 µs
Pulse energy	~ 0.5 Joule	~ 0.5 Joule	~ 2 Joule
Pulse repetition rate	~ 0.1 s^{-1}	~ 0.1 s^{-1}	~ 0.5 s^{-1}
Transmitted beam width	< 1 mrad	< 1 mrad	< 1 mrad
Transmitter efficiency (estimated)	~ 75%	~ 75%	~ 75%
Aperture of receiving telescope	40 cm	30 cm	40 cm
Receiver efficiency (estimated)	~ 30%	~ 30%	~ 30%
Quantum efficiency of photodetector	~ 5%	~ 5%	~ 5%
Bandwidth of receiver filter	20 Å	3 Å	6 Å

Table 1: Technical features of the ~~lidar instruments~~lidars operated at Lexington and College, Fairbanks.

~~An additional set of relevant features of~~ A problem with these early Ruby lasers was the ~~instrument follows. The~~ fluorescent emission ~~after~~which followed the laser pulse ~~has been emitted, was prevented incorporating~~. These lidars incorporated a ~~small~~ rotating shutter ~~into~~in the transmitting unit, synchronized with the Q-switching ~~device~~. The sensing unit for the backscattered signal consisted ~~in~~of an astronomical telescope, with an interference filter and ~~a~~ photomultiplier tube synchronized to another rotating shutter, to avoid ~~its expositon~~exposure to the intense returns from short distances. The photomultiplier was cooled with methanol and dry ice, to reduce the ~~levels of its~~ dark current (**G-66**).

2.2 Lidar measurements:

Lidar observations were conducted at Lexington, Massachusetts (42° 25'N, 71° 15'W) and ~~also~~ at College, (64° 53'N, 148°3'W) located in the city of Fairbanks, Alaska, hereinafter identified as Fairbanks. The measurements were supported by the NASA Grant NGR-22-009-131. One of the semi-annual reports ~~mention~~mentions more than 100 measurements conducted (Fiocco, 1966a). However the ~~amount~~number of ~~total~~ profiles appearing in Grams PhD dissertation was 75. Nine days of measurements from July 26 to August 21, 1964, were conducted in Fairbanks. At Lexington, Massachusetts, 23 days of measurements from January 14 to May 20, 1964, and 43 days from October 11, 1964 to July 21, 1965 were made. At both sites, measurements were ~~conducted at night~~restricted to ~~avoid~~dark nighttime conditions. A single laser shot was registered by photographing the ~~contribution of daylight~~return signal on an oscilloscope covering up to ~~the~~40 km, and then digitized by hand. The digitized return signals ~~registered by the photomultipliers.~~from a set of laser shots were then averaged in 1 km bins (**G-66**; **GF-67**).

Tabla con formato

~~The lidar signal returns at both sites were registered photographically from oscilloscopes covering up to 40 km and then digitized. Then the digitized lidar return signals from a set of daily laser shots were averaged in 1 km bins (G-66; GF-67).~~

2.3 Backscattering ratios in the original lidar dataset:

It is well known that solving the lidar equation for the single ~~-~~ wavelength elastic lidar is an ill-posed problem. The ~~single~~ returned signal, is the result of ~~two main species,~~scatter from both molecules and aerosol particles, ~~making it necessary to the use of~~hence additional information ~~to estimate the solution (eg,~~is necessary to separate their contributions (e.g., Kovalev, 2015). ~~That is the reason why still today processing single wavelength lidar profiles remains a challenge.~~ Considering this fact, we may understand the magnitude of the challenge confronted by Prof. ~~Girogio~~Giorgio Fiocco and then BSc Gerald W. Grams, Prof. Fiocco's PhD student, when they conducted the processing of the first ever set of lidar returned signals from stratospheric aerosols.

~~We now~~ First, we describe the procedure applied in **G-66** to derive ~~SR(~~the backscattering ratio (SR(694, z~~)~~)). The average photoelectron flux registered by the photomultiplier, which is proportional to the backscattered signal, that was represented by the ~~expression~~Eq. (3.8) in **G66**;

$$\frac{dn(z)}{dt} = K \frac{\sim\!\!N_A(z)\sim\!\!}{\sim\!\!z^2\sim\!\!} \frac{\sigma_T(z)}{z^2} \qquad (1)$$

Where z is the altitude, ~~n~~$_z$n(z) is the number of photons at the altitude z, ~~N$_A$ is the molecular number density~~σ_T(z) the total radar cross-section per unit volume of atmospheric constituents at ~~altitude~~ z~~, obtained from the US 1962 Standard Atmosphere~~. K is a constant resulting from all the terms not depending on the altitude in the optical radar equation, including T_{2w}^2 , the two-way atmospheric transmittance (see **G-66** for more details). The assumption of a constant value for T_{2w}^2 in the stratosphere was based on the atmospheric attenuation model proposed by Elterman (1964). The model provided magnitudes of the molecular and aerosol scattering, and the ozone absorption, showing that almost all attenuation of the laser ~~bean~~beam occurs in the troposphere. The model ~~allowed~~gave an estimate ~~at 700 nm~~ of the variability of the term T_{2w}^2 , at 700 nm in the stratosphere, between 10 and 30 km which was below 3%. The correction of the returned signal, associated with the two ~~-~~way transmittance of the laser beam throughout the atmosphere, was then neglected and it was assumed that the atmospheric ~~attenuation term was constant~~extinction term was constant. This is a good assumption for times of low stratospheric aerosol loading. For enhanced stratospheric aerosol, e.g. after volcanic eruptions, however, aerosol extinction becomes important, reduces the stratospheric transmission, and makes it range dependent.

The returned signal from a set of laser shots was averaged in time and in altitude to a resolution of 1 km between 12 and 30 km. Next, the ratios between the averaged signal at each level and the values at the same level of the right side of the equation (1) were calculated for each profile between 12 and 30 km. A final step for each profile consisted in normalizing the ratios calculated in each profile between 12 and 24 km~~. To that end, for each profile~~, with the average ~~value~~ratios between 25 and 30 km ~~of~~producing the ~~ratios calculated in~~derived SR(694, z) under the ~~former step were determined. Then for each profile the ratios in the altitude range 12 and 24 km were divided by the average value of the ratios between 25 and 30 km from the same profile. The resulting values were considered to be the backscattering ratio (SR$_\lambda$(λ, z)): the ratio between the total (aerosols + molecules) backscattering divided by the molecular backscattering~~.assumptions already cited. The normalization procedure ~~assigned the backscattering ratio to be equal to one above 25 km, after assuming~~assumed the contribution from aerosols was negligible ~~compared to the molecular at those levels. This assumption would lead~~above 24 km, leading to an under-estimate of stratospheric aerosol since there would have been aerosol at these altitudes (Russell, et al., 1979).

The ~~SR$_\lambda$(λ,~~SR(694, z) derived from the lidar measurements conducted at Lexington and Fairbanks were reported in tabular format in the Gerald W. Grams PhD Thesis (**G-66**), and cited in the acknowledgements section of **GF-67**. It was the unique reference of its existence, the clue that guided us in our search for the lidar measurements.

Con formato: Fuente: 11 pto
Con formato: Fuente: 11 pto
Con formato: Fuente: 11 pto
Con formato: Fuente: 11 pto
Con formato: Centrado

2.4 ~~Algorithm and complementary datasets~~Algorithms used in the processing:

~~Far beyond the mere rescue and deposit on public repositories of datasets, mainly from stratospheric aerosols from past volcanic eruptions from the 60's to the present, the~~The SSiRC Data Rescue Activity is committed, whenever it will possible, to re-calibrate each dataset and determine its levels of uncertainties (SSiRC, 2020). Because some stratospheric aerosol lidar datasets have already been identified and located, we ~~consider that its recalibration or reprocessing should be conducted~~endeavor to reprocess them using a standardized algorithm, to guarantee the best possible ~~consistence~~consistency among the different lidar datasets. ~~To contribute to this task~~ Below, we describe ~~below~~ the processing algorithm ~~we used~~ as a first step in that direction.

The lidar backscattering ratio (SR(λ, z)) is commonly defined as the ratio between the total backscatter ($\beta_T(\lambda, z)$) and the molecular backscatter $\beta_m(\lambda, z)$, at the altitude z and wavelength λ. $\beta_T(\lambda, z)$ is the sum of $\beta_m(\lambda, z)$ and the aerosol attenuated backscatter ($\beta_a^A(\lambda, z)$). That definition is ~~associated~~related to the fact that in the retrieval of $SR_o(z)$ the two-way total transmittance(T_T^2) correction was neglected (~~Hosteler~~Hostetler et al., 2006):

$$SR(\lambda, z) = \left\{\frac{\beta_{m}(\lambda,z)+\beta_a^A(\lambda,z)}{\beta_{m}(\lambda,z)}\right\}\frac{\beta_m(\lambda,z)+\beta_a^A(\lambda,z)}{\beta_m(\lambda,z)} \quad (2)$$

$\beta_m(\lambda, z)$ is derived using the equation:

$$\beta_m(\lambda, z) = \frac{\sigma_m(\lambda,z)}{S_m} = \frac{3\ \sigma_m(\lambda,z)}{8\ \pi} \quad (3)$$

where $S_m = (8\pi/3)k_{bw}$ is the molecular extinction to backscatter ratio for the molecular scattering, commonly approximated by 8π/3 (Collins and Russell, 1976) after neglecting the dispersion of the refractive index and the King factor of the air represented by k_{bw}. The volume molecular scattering coefficient, $\sigma_m(\lambda, z)$ is determined by the equation:

$$\sigma_m(\lambda, z) = \frac{N_A\ Pr(z)}{R_a Temp(z)}\ Q_s(\lambda) \quad (4)$$

Where $N_A = 6.02214\times10^{23}$ (1/mol) is Avogadro's number; Ra = 8.314472 (J/K/mol) is the gas constant and Qs(λ) the total molecular scattering cross section per molecule for the standard air. The derived equation for Qs(λ) for standard air is (Hostetler et al., 2006):

$$Q_s(\lambda) = 4.5102\ \times 10^{-27}\ \left[\frac{\lambda(nm)}{550}\right]^{-4.025-0.05627\times\left[\frac{\lambda(nm)}{550}\right]^{-1.647}} \quad (5)$$

~~Then from~~From equation 2 ~~we retrieved~~ β_a^A:

$\beta_a^A(\lambda, z)$~~, using the expression:~~

$$\beta_a^A(\lambda, z) = (SR_o(z) - 1)\beta_m = (\ SR(694, z) - 1)\ \beta_m(\lambda, z) \quad (6)$$

To derive the aerosol backscatter profiles at 532 nm ($\beta_a(532, z)$~~)~~), we used the wavelength exponents (kb(z, t)) for aerosol backscatter in the range of wavelengths between 532 and 694 nm derived for the stratospheric aerosols produced by the 1991 Mt Pinatubo eruption (Jäger and Deshler, 2002) according to the expression:

$$\beta_a(532, z)\ =\ \left[\frac{532}{694}\right]^{kb(z,t)}\ \frac{\beta_a^A(694,z)}{T_m^2(694,z)\ T_{O3}^2(694,z)} \quad (7)$$

~~Applying in addition the corrections for, T_m^2~~Next, we calculated $T_m(694, z)$ and ~~$T_{O3}^2(694, z)$~~ $T_{O3}\ (694, z)$, the two-way molecular and ozone transmittances at λ = 694 nm, to ~~the~~correct $\beta_a^A(694, z)$. The ~~generic~~general definition of the two-way ~~tansmittance~~transmittance is:

$$T_j^2\ T_j(\lambda, z) = e^{-2\int_{sup}^{z}\alpha_j(\lambda,z)dz} \quad (8)$$

~~With~~with the ~~sub~~ index j representing in $\alpha_j(\lambda, z)$ the vertical profiles of the ~~scattering~~extinction by ~~the~~ molecules $\alpha_m(\lambda, z)$), ozone ($\alpha_{O3}(\lambda, z$~~)))~~, and aerosols ($\alpha_a(\lambda, z)$).

~~Then the~~The aerosol extinction ($\alpha_a(532, z)$) is calculated by the expression:

$$\alpha_a(532, z) = EB_c(z, t)\ \beta_a(532, z) \quad (9)$$

Con formato: Centrado

Con formato: Centrado

Con formato: Centrado

Con formato: Centrado

Con formato: Centrado

Con formato: Sangría: Izquierda: 0 cm

Con formato: Centrado

Con formato: Centrado

where ~~BE,~~EB$_s$(z, t) are the altitude and time dependent backscattering to extinction conversion coefficients from λ = 694 nm to λ = 532 nm also derived for ~~the~~ Mt Pinatubo (Jäger and Deshler, 2003).

Finally we derive the ~~aerosols~~aerosol scattering corrected by the total two-way transmittance ($\alpha_a^{Ta}(532,z)$~~)~~), by applying the correction ~~by~~for the two-way aerosol transmittance $T_a^2(z)$

$$\alpha_a^{Ta}(532,z) = \frac{\alpha_a(532,z)}{T_a^2(532,z)} \frac{\alpha_a(532,z)}{T_a(532,z)} \qquad (10)$$

Con formato: Centrado

Because the information available to calculate ~~the~~ $T_a^2 T_a(532,z)$ should be determined ~~from~~using the total aerosol optical depth (TAOD) measurements from sun photometers we applied a two-step procedure. The first step consists of using the TAOD to calculate a first guess ~~$T_a^2(532,z)$ followed by the~~, $T_a(532)$, which is a unique value for all the altitudes. It is follow by calculation of a first guess $\alpha_a^{Ta}(532,z)_*$ profile. Then the stratospheric AOD (sAOD) is calculated integrating $\alpha_a^{Ta}(532,z)_*$ between 12 and 24 km. The second step calculates~~:~~ (see Suplement-1 for details on the calculations of TAOD):

$$tAOD = TAOD - sAOD \qquad (11)$$

Con formato: Centrado

~~and the calculation of $T_a^2(532,z)$ is repeated but using tAOD instead of TAOD~~producing a profile of $T_a(532,z)$ with the particularity of having a constant value of $T_a(532)$ from the surface to 11 km, and then a profile of $T_a(532,z)$ between 12 and 24 km. This profile of $T_a(532,z)$ is applied in equation (11) getting the definitive values of $\alpha_a^{Ta}(532,z)$.

The algorithms for the solution of the single wavelength lidar equations apply the two-way transmittance correction to the raw lidar returned signal, together with squared distance correction, ~~well~~ before the backscattering ratio is calculated. In our case the available information we have ~~are~~ the backscattering ratios which have been derived without conducting the two~~-~~way transmittance correction (**G-66**~~).~~) for any species. That is the reason that correction was included in the retrieval of $\beta_a(694,z)$ in equation (7). However only the molecular and ozone two way transmittance corrections (~~$T_m^2(694,z)$~~ $T_m(694,z)$, ~~T_{O3}^2~~ $T_{O3}^{\frac{2}{\cos\theta}}(694,z)$) were included in this step.

Con formato: Fuente: 11 pto

Con formato: Fuente: 11 pto

The aerosol two-way transmittance correction, ~~T_a^2~~ $T_a(532,z)$, was delayed until the final step to derive $\alpha_a^{Ta}(532,z)$. The reason was that the available information on the AOD was at λ = 500 nm and it was the total AOD, including the sAOD that we are ~~trying~~attempting to retrieve. ~~No~~ Ångstrom exponent contemporary information for the Agung eruption in the eastern US in the range 500 to 694 nm was not found. ~~Using~~Hence, we use the Ångstrom ~~exponent climatological values~~exponents covering the cited wavelength range from 1995 to 2019 from the nearest Aerosol Robotic Network (AERONET, 2020) stations ~~we derived~~, we converted the total AOD at 500 nm to 532 nm ~~only, because it was~~. With a ~~very near λ. It was the solution to~~ lack of trusted information ~~with~~, the aim was to minimize the error that could be introduced for converting the AOD to 694 nm. ~~There have been abundant accounts about the changes~~Changes of the aerosols physical~~-~~ and chemical properties ~~of aerosols in the eastern US~~ from the sixties until the present in the eastern US has been documented (Went, 1960; Husar et al., 1991).

2.5 Complementary datasets used:

The correction for the attenuation of the lidar signal by the two-way transmission by atmospheric molecules, ozone and aerosols is often considered negligible and ignored, based on signal to noise ratio considerations or for simplicity ~~as it was the case in the original processing of these set of measurements (~~(e.g. **G-66**; **GF-67**). We were motivated to make that correction by the fact that~~, during a little more than half a century,~~ the accuracies of the different instruments available for measurements of the stratospheric aerosols from the 1963 Mt. Agung eruption ~~have been~~are still under, ~~still unsettled,~~ scrutiny and discussions (~~exc~~e.g., Deirmendjian, 1965; Dyer, 1971a; Clemesha, 1971; Dyer, 1971b; Deirmendjian, 1971; Stothers, 2001; Timreck et al., 2018). Our goal was to produce the ~~most accurate~~consistently processed aerosol extinction and optical depth from the rescued measurements, based on the contemporary state of the art measurements in the sixties of the XX century. The different data sources, and processing algorithms, we calculate the two-way transmittance corrections

by atmospheric molecules, ozone and aerosols as described in Supplement 1.

Table 2 summarize the locations of the sites where radiosonde, ozone soundings and atmospheric turbidity measurements were conducted. Also the distances from each individual site to the corresponding lidar site are provided. Following each individual dataset is described.

Table 2: Locations of the observation sites where thermodynamic variables and ozone vertical soundings were measured nearby College, AK and Lexington, MA. Also the site of the atmospheric turbidity measurements is listed. The last column list the distances to Lexington (*) and to Fairbanks(**).

Station	**Variable**	**Latitude**	**Longitude**	**Elevation**	**Dist.**
Nantucket, MA*	Temp, Pr	41.2°N	70.0°W	14 m	162.1 km
Bedford, MA*	O_3	42.5°N	71.3°W	251 m	10.7 km
Blue Hill Obs., MA*	TAOD 500 nm	42.2°N	71.1°W	192 m	24.1 km
CARTEL, Canada*	TAOD 500 & 675 nm	45.38°N	71.93°W	251m	334.4 km
Fairbanks, AK **	O_3, Temp, Pr,	64.8°N	147.9°W	353 m	11.7 km
Fairbanks, AK**	TAOD 500 nm	64.86°N	147.85°W	133 m	9.8 km
Bonanza Creek, AK**	TAOD 500 & 675 nm	64.74°N	148.32°W	353m	23.6 km

2.5.1 Datasets used to estimate the thermodynamic local variables:

To derive $\beta_m(\lambda, z)$, $\alpha_m(\lambda, z)$, $\alpha_a(\lambda, z)$ and $T^2_{itt}(z)$ the required variables are the temperature (Temp(z)), pressure (Pr(z)) and molecular number density ($N_d(z)$). We used the vertical profiles of Temp(z), Pr(z) and $N_d(z)$ from the 1962 US Standard Atmosphere (U. S. Standard Atmosphere, 1962).

We also made use of the Temp(z) and Pr(z) profiles (deriving $N_d(z)$) from the most complete and nearest sounding station. In the case of the soundings we took into account the fact that lidar observations were performed at night, typically near 21:00 EST (**G-66**; **GF-67**), then we selected Temp(z) and Pr(z) profiles from nearby soundings stations conducted at 00 GMT from the Integrated Global Radiosonde Archive (IGRA) Version 2 database (Dumre et al., 2016). **G-66** and **GF-67** mention the contemporary Bedford, MA, soundings near Lexington but although a total of 731 temperature profiles from this site are available in digital format (IGRA – 2, 2020) they only cover 1943 to 1945. The information about the temperature profiles from the ozone soundings from 1963 to 1964 exists, but it is plotted on the ozonogram reports (Hering and Borden, 1965).

For Lexington, Massachusetts (42° 25'N, 71° 15'W) we used the soundings from the station at Nantucket (41º 15' N, 70º 4' W, 14 m asl), code USM00072506, located at 163 km and around 1º of latitude south. Because the altitude of interest is between 12 km and 24 km, the upper troposphere and lower stratosphere in this region, they could be considered more representative than the US 1962 Standard Atmosphere. For Fairbanks, Alaska (64° 53'N, 148°3'W) we used Fairbanks (64º 49'N, 147º 53'W, 134 m asl), code USM00070261, at a distance of 11 km. They are the nearest sounding stations in IGRA-2 with Pr(z) and Temp(z) profiles during 1964 and 1965. We used the soundings conducted the next day at 00 GMT because the local time at Nantucket, MA and Fairbanks, AK are -4 and -8 hours respect to GMT. At Nantucket, no sounding was available the next day at 00 GMT in 2 of the 66 measurements days. In those 2 cases, the same day 12 GMT sounding were used. The few gaps in Temp(z) and Pr(z) in both sets of data below 25 km were filled with the mean Pr(z) and Temp(z) profiles derived from all 1964 and 1965 Nantucket and Fairbanks daily Temp(z) and Pr(z) profiles at 00Z.

2.5.2 Datasets used for the estimation of the ozone 2-way transmittance:

We used the $N_{O3}(z)$ from the 1966 US Standard Atmosphere Supplement (COESA, 1967). In addition, we used the seasonal means of $N_{O3}(z)$ between 1963 and 1967 from ozone soundings conducted at L. G. Hanscom Fla., Bedford, MA and

Fairbanks, AK for Lexington and Fairbanks respectively (Hering and Borden, 1967).

The profile of the ozone absorption coefficient at a given wavelength ($k_{O3}(\lambda, z)$) is calculated using the profile of ozone cross sections ($\sigma_{O3}(\lambda, Temp(z))$):

$$k_{O3}(\lambda, z) = \sigma_{O3}(\lambda, Temp(z)) \times N_{O3}(z) \quad (12)$$

at the temperature (Temp(z)), where $N_{O3}(z)$ is the number density of ozone. The $\sigma_{O3}(\lambda, Temp(z))$ at λ = 694 nm is provided by Serdyuchenko et al., (2014) in the temperature range 193 to 293 ºK. We used the average of $\sigma_{O3}(\lambda, Temp(z))$, 9.88e-22 cm^2 $molecules^{-1}$, considering that the standard deviation of this averaging profile represents 2.4 % variability of the average value. This set of absorption coefficients have been recommended by the recent status report from the International Ozone Commission from WMO (Orphal et al., 2016).

2.5.3 *Datasets used for the estimation of the tropospheric aerosol 2-way transmittance:*

For Lexington we found contemporary statistics of turbidity measurements (**B**) at λ = 500 nm. Those measurements were part of the turbidity network established in 1961 by the U. S. Weather Bureau Research Station (later National Center for Air Pollution Control), Cincinnati, Ohio. For Lexington, the measurements were conducted at Blue Hill Observatory, Boston, Ma, 24 km from the lidar location. The Blue Hill Observatory frame plot with the monthly means for the period 1961 to 1966 are in figure 3 in Flowers et al., (1969). The curve of the monthly mean **B** belonging to Blue Hill Observatory in the frame plot on the figure were digitized (WebPlotDigitize, 2020). Then TAOD at λ = 500 nm was calculated using the equation (Volz, 1969), resulting from converting the decadic logarithm used to define **B** to the neperian logarithm used for AOD:

$$\mathbf{B} = 0.434 \times TAOD \quad (13)$$

For Fairbanks we did not find contemporary measurements, but there were manually conducted measurements in several places in the Arctic and Antarctic, including at Fairbanks (64.86°N, 147.85 °W, 133 m), with sun photometers at several wavelengths (Shaw, 1982). Those measurements are reported to be corrected by the molecular scattering and gas absorption (Shaw et al., 1973). The instruments were calibrated at Mauna Loa Observatory using Langley method with root mean square errors (RMSE) of sun photometer voltage output readings (V) of $\frac{\delta V}{V} \approx 10^{-3}$ having a systematic RMSE for AOD = +/- 0.002 and the total error estimated as +/- 0.004 (Shaw, 1982). At Fairbanks the annual mean AOD = 0.110 from 105 observations at λ = 500 nm is reported on table 1 of the cited reference, but also the AOD annual cycle appears in the lower panel of figure 2, showing the high AOD values in late winter and spring, peaking up to 0.135. We then digitized the mean AOD and its variation range values for July (no data for August appears on the figure), resulting AOD = 0.082 ± 0.022. Although Shaw (1982) does not provide the information of the year the measurements were conducted this data is cited and cited to have been conducted in 1978 by Freund (1983).

We also used AOD data at 500 nm from the 2 nearest AERONET stations to each site having long-term records. Bonanza Creek, AK, is less than 30 km from the location the lidar measurements were reported to be conducted at Fairbanks. TAOD measurements at this site have been conducted from 1997 to the present. The other site belongs to the Centre d'Applications et de Recherches en Teledetection (CARTEL), at the Universite de Sherbrooke, Canada, 334 km from Lexington.

From both sites we also used the climatological monthly means of TAOD at 500 and 675 nm from 1997 to 2019 for Bonanza Creek, and 1995 to 2019 for CARTEL (AERONET, 2020). We then derived the TAOD at 532 nm using the Ångstrom exponents calculated from the TAOD climatological monthly means for the interval 440 to 870 nm,that we used for Lexington. In the case of Bonanza Creek, we had one "contemporary" value from July 1978 (Shaw, 1982), and we selected the July climatological monthly mean, as the "current" value. After the conversion to 532 nm they were respectively 0.087and 0.242, and we used the same value for both July and August 1964 lidar measurements at Fairbanks.

~~In the case of Lexington, for comparison purposes, we digitized the average monthly mean TAOD for 26 Eastern US stations from 1972 to 1975 from Husar et al., (1981). The series of monthly mean TAOD values were converted from 500 nm to 532 nm, with the procedure described above, using the Ångstrom exponents for the interval 440 to 870 nm. The figure 1 shows the resulting values. The high TAOD values for the two series before the 1960s and 1970s are representative of what have been reported for the Eastern US (Husar et al., 1991). The natural conditions contribute to an elevated background AOD attributed to the combination of absolute and relative humidity, and the vegetation density, both of which could be responsible for increased natural aerosols either from hygroscopic marine aerosols or from secondary aerosols originating from vegetation (e.g. Went, 1960). Additionally an important contribution to the TAOD came from anthropogenic aerosols originating from the extensive use of fossil fuels in the region. In fact, as their figure 1 shows, the pollution increased with respect to the 1960s (Husar et al., 1991). Recent research reports aerosol simulations for the historical period from 1850 to 2014 using the GISS ModelE2.1 with two different aerosol schemes to contribute to the Coupled Model Intercomparison Project Phase 6 (CMIP6). The simulations result in the AOD showing an increasing trend from well before 1900 until the early 1970s in the Eastern US, supporting the AOD data features we collected from Blue Hills Observatory (Bauer et al., 2020).~~

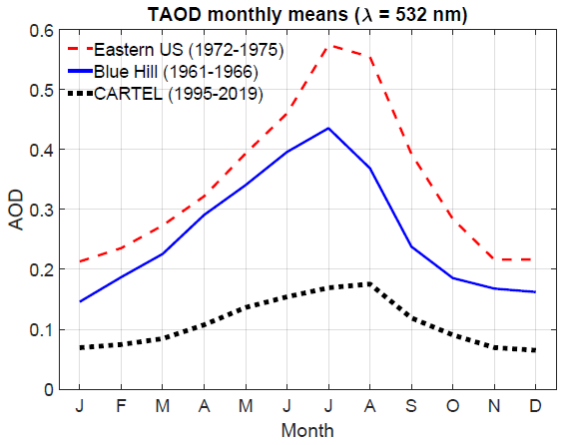

~~**Figure 1: Contemporary and current TAOD monthly means at 532 nm from Blue Hill Observatory, MA, from 1961 to 1966, the average of 26 stations in Eastern US between 1972 and 1975 and CARTEL, Canada, from 1995 to 2019.**~~

2.6 Numerical and statistical methods:

For each of the two datasets we ~~calculated the statistical results of the~~calculate percentage differences ($\Delta\alpha_{*US}$) between $\alpha_a(532,z)_{US}$ calculated using the same β_m~~(594, z)~~$(694, z)$ profile from the 1962 US Standard Atmosphere for all the days and the $\alpha_a(532,z)_*$ calculated using the β_m(~~594~~$694, z)$ profiles derived from the daily soundings:

$$\Delta\alpha_{a*} = \alpha_a(532,z)_{US} - \alpha_a(532,z)_* \qquad (~~14~~12)$$

and the percent differences $\Delta\alpha\%_{a*}$ by the expression:

$$\Delta\alpha_{a*}\% = \left[\frac{\alpha_a(532,z)_{US} - \alpha_a(532,z)_*}{\alpha_a(532,z)_{US}}\right] \frac{\alpha_a(532,z)_{US} - \alpha_a(532,z)_*}{\alpha_a(532,z)_{US}} \times 100 \qquad (~~15~~13)$$

Similarly we defined the differences $\Delta\alpha_{at2w}$ and the percent differences $\Delta\alpha_{at2w}\%$ between the $\alpha_a(532,z)_*$ calculated using the β_m~~(594, z)~~$(694, z)$ profiles derived from the daily soundings, and its corrected values $\alpha_a(532,z)_{t2w}$ resulting for accounting for the two-way atmospheric transmittance.

Also~~ we defined~~, for cumulative aerosol optical depth in the layer 12 to 24 km, we define $\tau_a(532,)_*$ and $\tau_a(532,z)_{US}$ calculated from the $\alpha_a(532,z)_*$ and $\alpha_a(532,z)_{US}$ respectively:

Con formato: Centrado

Con formato: Centrado

$$\Delta\tau_{a*} = \tau_a(532,z)_{US} - \tau_a(532,z)_* \qquad (\text{~~16~~}14)$$

and the percent differences $\Delta\tau\%_{a*}$ by the expression:

$$\Delta\tau_{a*}\% = \left[\frac{\text{~~}\tau_a(532,z)_{US} - \tau_a(532,z)_*\text{~~}}{\text{~~}\tau_a(532,z)_{US}\text{~~}}\right] \frac{\tau_a(532,z)_{US} - \tau_a(532,z)_*}{\tau_a(532,z)_{US}} \text{ x } 100 \qquad (\text{~~17~~}15)$$

2.7 Relative Error estimates:

The present evaluation of the relative errors in the different processing steps of the single wavelength elastic lidar followed the algorithms developed by Russell (1979). Whenever it was possible we calculated the different terms of the equation based in the available dataset error. In several cases we combined information from the rescued metadata associated with the measurements and from available additional information in literature.

2.7.1 Backscattering ratio relative error:

~~As it was explained above, the data we rescue are a reasonable approximation of what we today know as the backscattering ratio described in equation (2). Then we~~We use the equation (19) from Russell (1979) quantifying the contributions from the different sources to the relative error in backscattering ratio $\frac{\delta SR}{SR}$:

$$\left(\frac{\delta SR}{SR}\right)^2 = \left(\frac{\delta N_s}{N_s}\right)^2 + \text{~~}\left(\frac{\delta T_{zw}}{T_{zw}}\right)^2\text{~~}\left(\frac{\delta T_T}{T_T}\right)^2 + \left(\frac{\delta\beta_m}{\beta_m}\right)^2 + \left(\frac{\delta\beta_{m*}}{\beta_{m*}}\right) - \left(\frac{C^2_{FF*}}{\beta_m\beta_{m*}}\right) + \left(\frac{\delta SR_{min}}{SR_{min}}\right)^2 \qquad (\text{~~19~~}16)$$

Where $SR(\lambda, z)$ is the total backscattering ratio; N_s is the signal measured; ~~T_{zw}~~T_T the two-way transmittance from aerosols; molecules and ozone; β_m the molecular backscattering; β_{m*} molecular backscatter at the normalization level; ~~SR~~$SR_{min}(\lambda, z)$ total backscattering ratio at the normalization level and C^2_{FF*} the covariance between measured β_m and β_{m*}.

For estimating the magnitude of the signal measurement error we rely on the information provided by **G-66**. He estimated statistical fluctuation of the signal, the shot noise of the photodetector and other sources on the order of 0.2 to 3%. ~~Then~~For both ~~for~~ Lexington and Fairbanks~~:~~ we assume $\left(\frac{\delta N_s}{N_s}\right) = 3\ \%$

As cited above, according to **G-66** if no ~~T_{zw}~~T_T correction was conducted then the term ~~$\left(\frac{\delta T_{zw}}{T_{zw}}\right)^2$~~ $\left(\frac{\delta T_T}{T_T}\right)^2 = 0$.

Because in the calculation of $SR(\lambda, z)$ ~~,~~ values of $N_d(z)$ from the 1962 US Standard Atmosphere were used (**G-66**~~)~~), it was assumed $\frac{\delta\beta_m(\lambda,z)}{\beta_m(\lambda,z)} = 3\ \%$ for both sites (e.g. Russell et al, 1979). In addition we assumed $\left(\frac{\delta\beta_m}{\beta_m}\right) = \left(\frac{\delta\beta_{m*}}{\beta_{m*}}\right)$, and $C^2_{FF*} = 0$ after assuming measurement errors are uncorrelated. ~~It is a plausible assumption because the profile~~The use at the lidar levels of interpolated β_m ~~used~~values from the lower resolution ones calculated using the US 1962 Standard Atmosphere ~~for the vertical resolution of the lidar~~, support the former assumption.

The term δSR_{min} was ~~evaluated~~calculated according to table (1b) in Russell (1979) for the $SR_{min} = 1.01$ and the respective latitudes of both sites. Then ~~for both sites, according to~~following Russell et al. (1979~~).~~), we assume

$$\delta SR_{min} = 0.07(SR_{max} - 1) \qquad (\text{~~20~~}17)$$

2.7.2 Aerosol backscattering relative errors:

The equation (18) in Russell (1979) to estimate the relative error in $\beta_a(694, z)$ can be approximated in our case by

$$\left(\frac{\delta\beta_a(694,z)}{\beta_a(694,z)}\right)^2 = \left(\frac{\beta_m}{\beta_a}\right)^2 \text{~~}\left\{(SR)^2\left[\left(\frac{\delta SR}{SR}\right)^2 + \left(\frac{\delta T_{zw}}{T_{zw}}\right)^2\right] + \left(\frac{\delta\beta_m}{\beta_m}\right)^2\right\}\text{~~} \text{~~}(21\left\{(SR)^2\left[\left(\frac{\delta SR}{SR}\right)^2 + \left(\frac{\delta T_T}{T_T}\right)^2\right] + \left(\frac{\delta\beta_m}{\beta_m}\right)^2\right\}\text{~~} \qquad (18)$$

The estimated error for the 2-way transmission corrections in Russell et al. (1979) provides the expression:

Con formato: Centrado

Con formato: Centrado

Con formato: Centrado

Con formato: Inglés (Reino Unido)

Con formato: Centrado

Con formato: Centrado

$$\left(\frac{\delta T_{2w}}{T_{2w}}\right)^2 \left(\frac{\delta T_T}{T_T}\right)^2 = 4\{[\delta\tau_a(\lambda,z)]^2 + [\delta\tau_m(\lambda,z)]^2 + [\delta\tau_{O3}(\lambda,z)]^2\} \quad (2219)$$

and considering the standard error of determinations of τ_a, τ_{O3}, and τ_m are respectively 50, 20 and 10% the following estimates are produced. That is: $\delta\tau_a = 0.5\ \tau_a$, $\delta\tau_{O3} = 0.2\ \tau_{O3}$ and $\delta\tau_m = 0.1\ \tau_m$. However, in our calculus chaincalculation of β_a, only the ozone and molecular two-way transmittances were used.

For this section of the procedure, we consideredconsider $\left(\frac{\delta\beta_m}{\beta_m}\right) = 10$% because we used radiosonde soundings at both sites (Russell et al, 1979).%. We neglected the error in computing Qs using equation (5) because its maximum relative error is 0.2 % for a spectral region of 350-1600 nm (HostelerHostetler et al., 2006), well below the errorerrors in $\left(\frac{\delta\beta_m}{\beta_m}\right)$.

Next we determined the relative error in $\beta_a(532,z)$ associated with the conversion from $\beta_a(694,z)$ in equation (7), using the wavelength exponents (kb(z, t)) for aerosol backscatter in the range of wavelengths between 694 and 532 nm (Jäger and Deshler, 2003). The errors were estimated from their figure 1 with $\left(\frac{\delta kb}{kb}\right)^2 = 10$ %:

$$\left(\frac{\delta\beta_{a(532,z)}}{\beta_a(532,z)}\right)^2 = \left(\frac{\delta\beta_a(694,z)}{\beta_a(694,z)}\right)^2 + \left(\frac{\delta kb}{kb}\right)^2 \quad (2320)$$

2.7.3 Aerosol extinction relative errors:

In the case of the α_a, its relative errors are:

$$\left(\frac{\delta\alpha_a}{\alpha_a}\right)^2 = \left(\frac{\delta\beta_a}{\beta_a}\right)^2 + \left(\frac{\delta EB_c}{EB_c}\right)^2 \quad (2421)$$

The last term in the right side represents the error in the EB_C for λ = 532 nm. In the case of the ones we used (Jäger and Deshler, 2002; 2003) the error has been estimated inat ± 40 % according to Deshler et al., (2003). For α_a^{Ta}, the aerosols extinction corrected by the aerosols two-way aerosols transmittance, using the estimates of its relative error described above:

$$\left(\frac{\delta\alpha_a^{Ta}}{\alpha_a^{Ta}}\right)^2 = \left(\frac{\delta\alpha_a}{\alpha_a}\right)^2 + \left(\frac{\delta T_{2wa}}{T_{2wa}}\right)^2 \quad (2522)$$

Using the cited set of equations and the assumptions described above we evaluated the error for each levelaltitude in each measurement.

3.0 Results:

3.1 Aerosols extinction cross sections and optical depth:

Figure 21 shows the $\alpha_a(532,z)$ cross-sectionscontours for Lexington. Panel a) $\alpha_a(532,z)_{US}$ is calculated using the same β_m(594,z)(694, z) profile from the 1962 US Standard Atmosphere for all the days; b) $\alpha_a(532,z)$, was calculated using and *B* the daily β_m(594,z)(694, z) profiles derived from the sounding at Nantucket, MA. On top of the figures we plotted the dates the measurements were conducted (red starts at 24.5 km level). In the case of Lexington the two dataIf measurement gaps higherare longer than 1 month, March, and July to September both in 1964, have been left blank in the cross-sections plots.. The temporal/vertical cross-sectioncontours of the aerosolsaerosol extinctions were generated using a linear time interpolation.

In general, the cross-sectionscontours show a high level of variability of the aerosol extinction for Lexington both in time and altitude associated with the complex thermodynamic processes in the upper troposphere-lower stratosphere of the eastern US.. Three main maximums are identified across the entire period. The first between 16 and 18 km at the beginning of the record in middle January 1964. The second between 14 and 16 km by November 1964 and the third at the same altitude but in the transition between March and April 1965. Evident is the decaying altitude of the maximums in time typical of the

Con formato: Centrado

Con formato: Centrado

Con formato: Centrado

Con formato: Centrado

volcanic aerosols clouds in the lower stratosphere. However, the occurrence of the absolute maximum at this time cannot be attributed to the volcanic aerosols from Mt Agung, ~~it~~as will be discussed below. No long-~~-~~term analysis of this type could be conducted on figure ~~3~~2 for Fairbanks because of the very short period of time it covers. However, the cross-section of $\alpha_a(532,z)_*$ for Fairbanks reveals ~~the~~ maximum values between 14 and 16 km with the absolute maximum around mid-August, ~~centred~~centered at 15 km. The magnitudes of $\alpha_a(532,z)_{US}$ in are slightly higher than the ones from $\alpha_a(532,z)_*$ for both sites, and it is also true for $\tau_{a\,US}$ and τ_{a*}. This is quantified in table 2. The magnitudes of the mean percent difference increase of both variables is around 1%.

~~Regarding the magnitudes of $\alpha_a(532,z)_{US}$ in figure 2, they are slightly higher than the ones from $\alpha_a(532,z)_*$. That is also the case in figure 3 showing the cross-sections for Fairbanks, with panels similar to figure 2.~~ This ~~is quantified in table 3. At both sites the mean and maximum values for $\Delta\tau_{a*}$ and $\Delta\alpha_{a*}$ are positive showing that the magnitudes of $\alpha_{a\,US}$ and $\tau_{a\,US}$ are in general higher than α_{a*} and τ_{a*}. Also in the table we appreciate that the magnitudes of the mean percent~~ difference ~~increase of both variables is around 1%.~~

~~The fact described above~~ disagrees with ~~the possibility~~ **G-66** ~~mentions about lower aerosol backscatter from the retrieval they conducted,~~where he found retrievals using the 1962 US Standard Atmosphere~~, and~~ slightly lower than the more realistic ones using soundings~~.~~, but the differences are within calculated errors. He arrived ~~to~~at that conclusion from "a cursory examination" of the local variations of molecular number density ($N_d(z)$) estimated with the Temp(z) profiles from ozone soundings at Bedford, MA (Hering and Borden, ~~1965).~~1967). He reported $N_d(z)$ variability rarely exceeded 5% of the $N_{dUS}(z)$ values at altitudes between 10 and 30 km.

Table ~~3~~2: Relative differences between the $\alpha_{a\,US}$ and α_{a*} as well as $\tau_{a\,US}$ and τ_{a*}

	Lexington				**Fairbanks**			
	$\Delta\alpha_{a*}$	$\Delta\alpha\%_{a*}$	$\Delta\tau_{a*}$	$\Delta\tau_{a*}\%$	$\Delta\alpha_{a*}$	$\Delta\alpha\%_{a*}$	$\Delta\tau_{a*}$	$\Delta\tau_{a*}\%$
Mean	1.89E-05	1.4	2.46E-04	1.2	1.42E-05	0.2	1.84E-04	1.6
|Mean|	5.92E-05	3.2	7.42E-04	3.3	1.85E-05	2.1	1.90E-04	1.7
Max	4.22E-04	42.2	2.71E-03	13.6	1.13E-04	6.4	4.30E-04	3.1

To estimate the effects of the differences between the magnitudes of $N_{dUS}(z)$ and $N_d(z)$ in the backscattering ratios we calculate the differences between the ratios defined by:

$$\Delta N_d(z) = \frac{N_{dUS}(z)}{M_{dUS}} - \frac{N_d(z)}{M_d} \qquad (~~18~~25)$$

~~The values in the denominators~~ M_{dUS} and M_d are the mean values of $N_{dUS}(z)$ and $N_d(z)$ between 25 and 30 km ~~respectively~~, replicating the procedure used by **G-66**. In figure ~~4~~3 the differences $\Delta N_d(z)$ for ~~all the~~ 66 soundings at Nantucket ~~used to calculate $N_d(z)$~~ and the 9 for Fairbanks are plotted. For Lexington, ~~on panel a), $N_{dUS}(z)$~~ $\Delta N_d(z)$ values are both negative and positive, but higher values of $N_{dUS}(z)$ dominate. ~~It is confirmed that the relative means and the maximum values of $\Delta\alpha_{a*}$ between the $\alpha_a(532,z)_{US}$ and $\alpha_a(532,z)_*$ for Lexington in table 3 are the same order of magnitude, 10^{-5} km^{-1} for the relative and absolute means and 10^{-4} km-1 for the maximum, larger than for~~For Fairbanks~~. The values of the relative means $\Delta\alpha_{a*}\%$ confirm the higher values when the 1992 US Standard Atmosphere is used, in contradiction with **G-66** estimation.~~ $N_{dUS}(z)$ always is greater.

~~It has been stablished that the~~The errors in lidar retrievals of $\alpha_a(532,z)_*$,attributed to the use of Temp(z) and Pr(z) from a model atmosphere to retrieve $N_d(z)$, are of the order of 3% and decrease to 1% when the source of Temp(z) and Pr(z) are soundings (Russell et al., 1979). Again in table ~~3~~2, the magnitudes of the absolute differences between the US 1962 Standard Atmosphere and the soundings at Lexington and Fairbanks for $\alpha_a(532,z)$ are in the order of 3~~%. That magnitude matches~~% agreeing with the error attributed if case models are used instead of soundings to derive $\beta_m(\lambda,z)$.

Con formato: Centrado

The figure ~~54~~ shows τ_{a*} both for Lexington (blue stars) and for Fairbanks (red diamonds). ~~Also figure 5 shows the monthly mean τ_a for the northen hemisphere (Sato et al., 1993).~~ The means for the entire period of measurements available at each site are 0.0215 and 0.0099 respectively. ~~The magnitude of~~Also shown is a monthly mean τ_a for the northern hemisphere (Sato et al., 1993). The mean τ_{a*} at Fairbanks ~~are~~is half that of Lexington, providing evidence of the decreasing aerosol amount with increasing latitude. ~~At the same time, some of the daily τ_{a*} values at Lexington are around the magnitude of the mean τ_{a*} at Fairbanks, because~~Because of the variability of $\alpha_a(532,z)_*$. ~~Few,~~ τ_{a*} values from ~~Lexignton have magnitudes near the values of~~ Lexington vary widely from the Fairbanks mean to the Sato ~~τ_a,~~magnitude, the current reference for this period. However, as we will see in the next section ~~a~~ better agreement is found when the measurements are corrected ~~by~~with two ~~-~~way transmittance attenuation.

Taking into account the ~~little~~small difference between the results using the US 1962 Standard Atmosphere ~~or~~and the soundings to derive $\beta_m(\lambda,z)$, the first simpler option ~~could~~can reliably be used. However we decided to use the soundings to minimize the errors and to capture the more realistic features of the aerosol cloud.

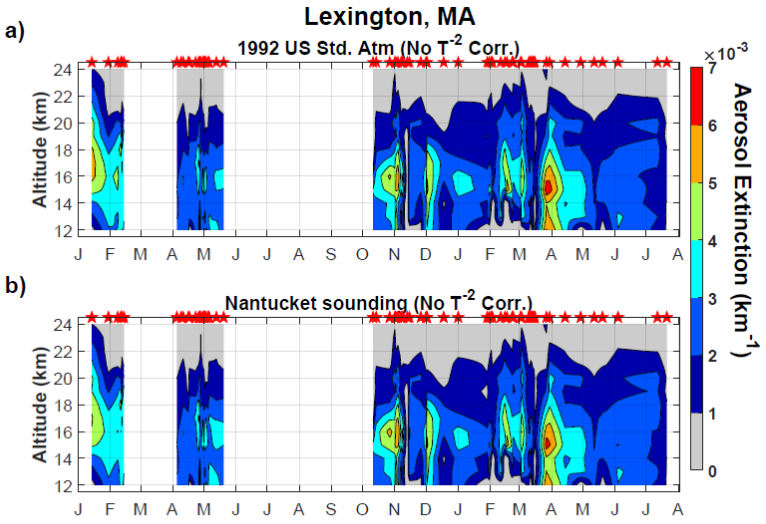

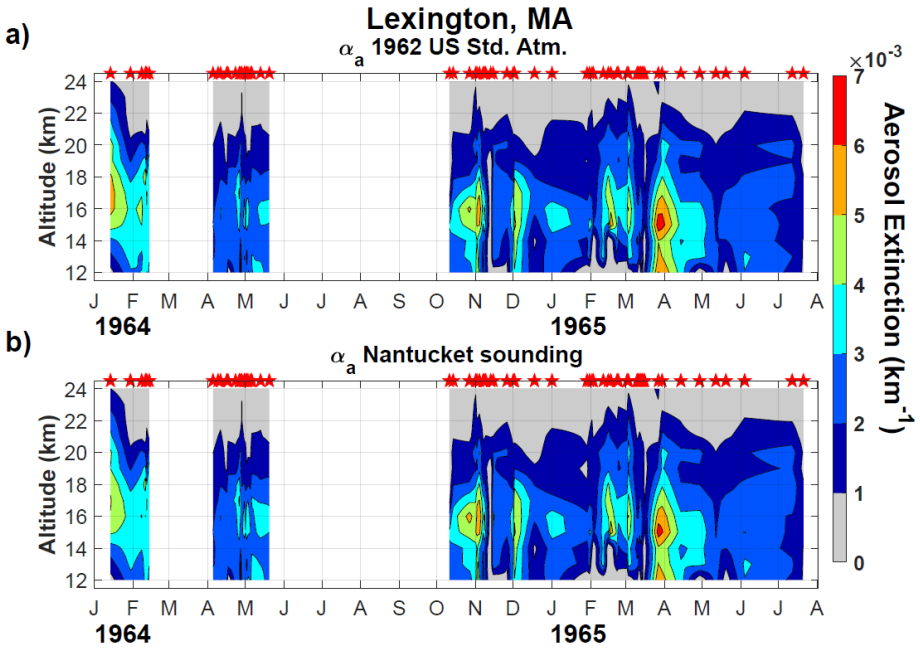

515 **Figure ~~2~~1: Panel a) $\alpha_a(532, z)$ calculated using the same β_m~~(594, z)~~$(694, z)$ profile from the 1962 US Standard Atmosphere for all the days; b) $\alpha_a(532, z)$ was calculated using the daily β_m~~(594, z)~~$(694, z)$ profiles from the sounding at Nantucket, MA. The red stars indicate the dates the measurements were conducted. The measurement gaps longer than 1 month, March, and July to September both in 1964, have been left blank.**

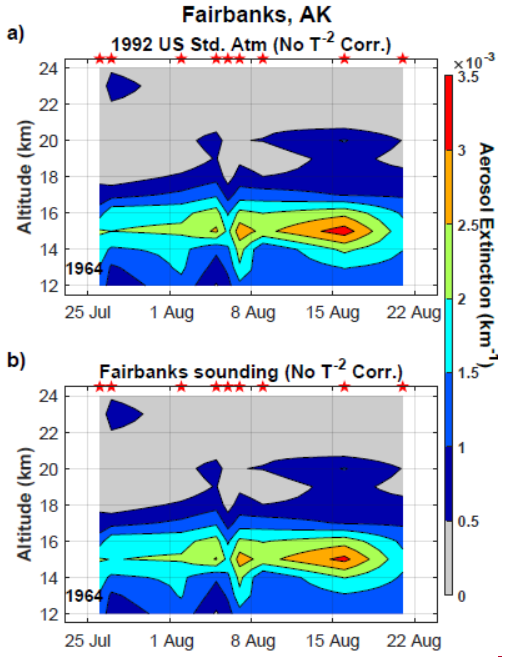
Fairbanks, AK
a)
1992 US Std. Atm (No T-2 Corr.)
b)
Fairbanks sounding (No T-2 Corr.)
Altitude (km)
Aerosol Extinction (km-1)
×10-3
1964
25 Jul
1 Aug
8 Aug
15 Aug
22 Aug

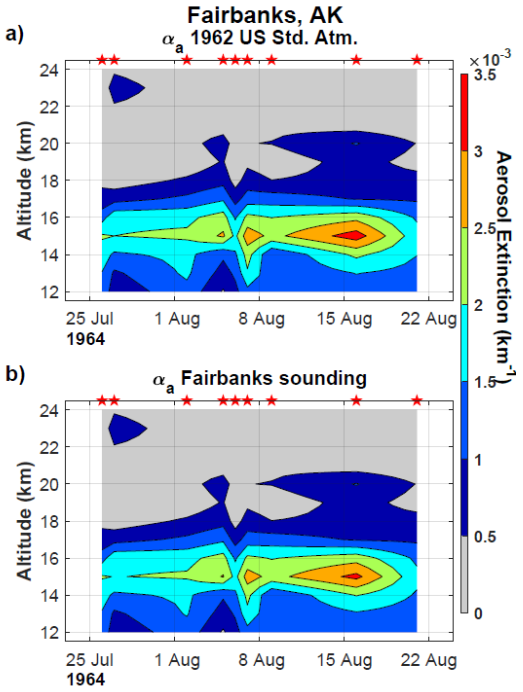
Fairbanks, AK
a)
αa 1962 US Std. Atm.
b)
αa Fairbanks sounding
Altitude (km)
Aerosol Extinction (km-1)
×10-3
1964
25 Jul
1 Aug
8 Aug
15 Aug
22 Aug

520

Figure ~~3~~2: Idem figure ~~2~~1, but for Fairbanks, AK.

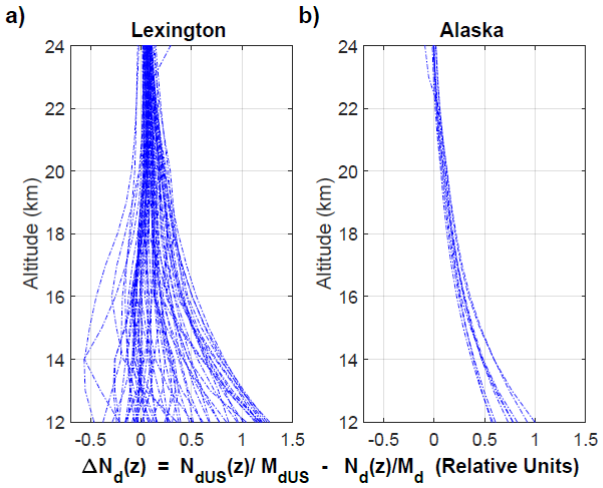

Figure ~~4~~3: Differences between the number molecular density (Nd (z)) from soundings and from the 1962 US Standard Atmosphere in the region from 12 to 24 km. Panel a) Represents N_d (z) from Nantucket soundings used for Lexington and b) N_d (z) from Fairbanks.

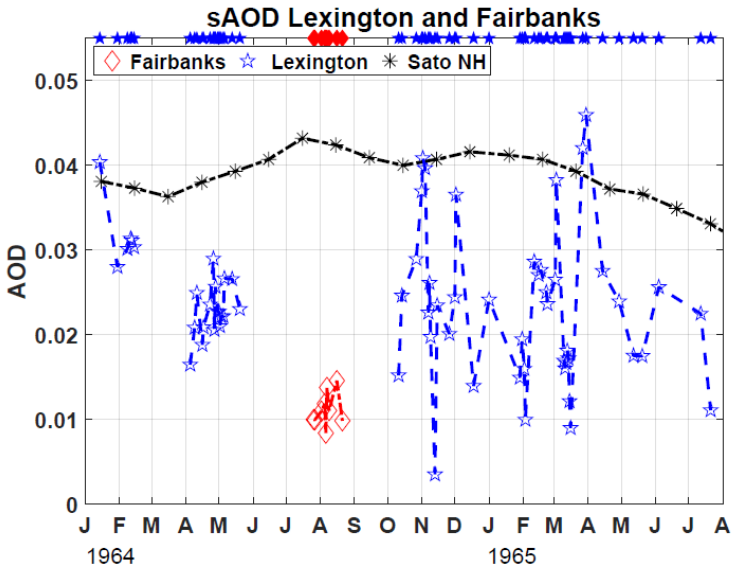

Figure ~~5~~4: Daily aerosol optical depth (τ_{a*}) for Lexington (blue stars), Fairbanks (red diamonds) and for the northern hemisphere (black asterisks) for the period the measurements were conducted. τ_{a*} was calculated from the $\alpha_a(532, z)_*$ derived using local soundings. Blue stars and red diamonds on the top axes of the figure are the dates the measurements were conducted.

3.2 Aerosols extinction ~~cross-sections~~contours and optical depth corrected by aerosol two-way transmittance attenuation:

Figure ~~6~~5 shows the ~~cross-sections~~contours of $\alpha_a(532,z)_*$ for uncorrected and corrected two-way transmittance ($\alpha_a^{Ta}(532,z)$) for Lexington. The initial values of TAOD were used to obtain a first estimate of $\alpha_a(532,z)_{*t2w}$. This $\alpha_a^{Ta}(532,z)_*$ is only used to calcuate sAOD for each day and is subtracted from TAOD to produce the tropospheric corrected value (tAOD) and the calculation is repeated to determine new profiles of the two-way aerosol transmittance and correct $\alpha_a(532,z)_*$ generating the$\alpha_a^{Ta}(532,z)$. Panel a) shows the ~~cross-section~~contour of uncorrected values of $\alpha_a(532,z)_*$, in panel b) the ~~cross-sections~~contours of $\alpha_a^{Ta}(532,z)$. The magnitudes of $\alpha_a^{Ta}(532,z)$ are higher than $\alpha_a(532,z)_*$. The two-way transmittance correction is dominated by the aerosols, in particular the tropospheric aerosols. The maximum extinction is at the third maximum, 1.071 x 10^{-2} km^{-1} located at 15 km, on March 27th 1965. Similarly in figure ~~7~~6, the Fairbanks ~~cross-sections~~contours for $\alpha_a(532,z)_*$ and $\alpha_a^{Ta}(532,z)$ show a notable difference in magnitude. ~~The~~Here the absolute maximum extinction occurred on August 16th 1964 at 15 km, with a magnitude of 3.8 x 10^{-3} km^{-1}.

Table ~~4~~3 contains the relative and absolute means and maximums for $\boldsymbol{\Delta\alpha_a^{Ta}}$, $\boldsymbol{\Delta\alpha_a^{Ta}}$%, $\boldsymbol{\Delta\tau_a^{Ta}}$ and $\boldsymbol{\Delta\tau_a^{Ta}}$% calculated using equations (14) to (17) respectively but for $\alpha_a(532,z)_*$ vs $\alpha_a^{Ta}(532,z)$ and $\boldsymbol{\tau_{a*}}$ vs $\boldsymbol{\tau_a^{Ta}}$. The magnitude of $\boldsymbol{\Delta\alpha_a^{Ta}}$ produced by the two-way transmittance correction is in the order of 10^{-3} km^{-1} for Lexington and 10^{-4} km^{-1} for Fairbanks~~. They represent~~, or an increase of ~~72 % in the first case~~67 % and 26 % ~~in the second~~respectively. These increases are due mainly to the two-way aerosol transmittances, dominated by the tropospheric AOD with magnitudes more than twice as high at Lexington than at Fairbanks. The increase in magnitude reveals more details of the vertical distribution of the $\alpha_a^{Ta}(532,z)$ and in the case of Lexington the presence of a 4th maximum during May 1964, who's vertical location matches the decreasing trend at the core of the stratospheric aerosols cloud.

In figures ~~8~~7 and ~~9~~8 the increases of $\boldsymbol{\tau_a^{Ta}}$. with respect to $\boldsymbol{\tau_{a*}}$ for Fairbanks and ~~for~~ Lexington ~~respectively~~ are shown~~:~~. At Lexington the $\boldsymbol{\tau_a^{Ta}}$.magnitudes are ~~around~~approximately the values of $\boldsymbol{\tau_a}$ from Sato et al., (1993) for the northern hemisphere ~~represented by the dot-dash~~ (black line~~, a)~~. This agreement is an important confirmation ~~that the results~~ of the ~~present study are in the accepted range of~~Sato magnitudes for $\boldsymbol{\tau_a}$ from Agung at the northern hemisphere. Again in table 3, the magnitudes of the increase of $\boldsymbol{\tau_a^{Ta}}$ are in the order of 10^{-2} for Lexington and 10^{-3} for Fairbanks, representing ~~a~~ 66 % and 26 % increases respectively.

At Lexington the absolute maximum value of $\boldsymbol{\tau_a^{Ta}}$, 0.~~076~~071 occurs on March 30th 1965, 3 days after the absolute maximum extinction was registered at 15 km. At Fairbanks the absolute maximum value of $\boldsymbol{\tau_a^{Ta}}$, 0.018, was registered on August 16th 1964, the same day the absolute maximum extinction was registered at 15 km at this site.

Table ~~4~~3: Idem than table ~~3~~2, but for the comparison of $\alpha_a(532,z)_*$ vs. $\alpha_a^{Ta}(532,z)$ and τ_{a*} vs τ_a^{Ta} See text for details.

	Lexington				Fairbanks			
	$\Delta\alpha_a^{Ta}$	$\Delta\alpha_a^{Ta}$%	$\Delta\tau_{at2w}$	$\Delta\tau_{at2w}$%	$\Delta\alpha_a^{Ta}$	$\Delta\alpha_a^{Ta}$%	$\Delta\tau_{at2w}$	$\Delta\tau_{at2w}$%
Mean	1.17E-03	67.2	1.52E-02	66.2	2.22E-04	26.5	2.89E-03	25.9
|Mean|	1.17E-03	67.2	1.52E-02	66.2	2.22E-04	26.5	2.89E-03	25.9
Max	3.60E-03	152.6	3.09E-02	148.8	8.35E-04	29.1	3.89E-03	26.7

~~During the course of more than two decades after~~Since the pioneering ~~stratospheric aerosols measurements with~~ lidar work by Fiocco and Grams (1964~~)~~), multiple researchers have contributed to the development of the processing algorithms to retrieve ~~aerosols~~aerosol optical properties and ~~its~~ errors (Russell et al, 1979, Klett, 1981; Klett, 1985, Kovalev, 2015). ~~Those facts~~These works explain the limitations ~~that do not allow the retrieval of~~on retrieving the full set of optical variables characterizing the stratospheric aerosols from the Fiocco and Grams dataset. However ~~using~~assuming a Junge size-

distribution model, and assuming Mie scattering with refractive index 1.5, they producedFiocco and Grams did produce estimates of the aerosol content of the stratosphere at 16 km: number concentration, surface area, and the aerosol density per unit volume of air. They also use the mean profile they derived to estimate the total of particles/cm^3, total surface area and a total mass, integrating the concentrations obtained between 12 and 24 km (**GF-67**). The only available optical property estimates, based inon some of the cited particle concentration estimates at 16 km and in the column, are the aerosol extinction at 16 km, (2 x10^{-3} km^{-1}) and the aerosol optical depth of (0.015), both at 694 nm (Deirmejian, 1971).

For comparing with the values reported above, we made estimates at of estimate $\alpha_a(694, z)$ from $\alpha_a(532, z)$ as well as $\tau_a(694, z)$ from $\tau_a(532, z)$ using the wavelength exponents for aerosols from Mt Pinatubo in the range of wavelengths 532 to 694 nm (Jäger and Deshler, 2002). We made the estimates for both for Lexington and Fairbanks because, as no clear assignation of the values cited above to one of the two sitescither site is made in **G-66** and **GF-67**. At the 16 km level, the mean value of $\alpha_a(694, z)$ was 10^{-3} km^{-1} for Fairbanks and 2 x 10^{-3} km^{-1} for Lexington matching for both sites the order of magnitude estimated by Deirmejian, (1971).

An additional validation of those results, in particular for $\tau_a^{Ta}(532, z)$ at Lexington appears in figure 9, where the stratospheric $\tau_a(532, z)$ for the northern hemisphere from January 1964 to July 1965 has been plotted (Sato et al., 1993). The magnitude of $\tau_a^{Ta}(532, z)$ is the same at Lexington (and also at Fairbanks, figure 8) as the $\tau_a(532, z)$ from Sato et al., (1993).

From 1963 to mid-1965, in addition to the 1963 Mt Agung, two other volcanoes were reported to have erupted in the northern hemisphere with Volcanic Explosivity Index (VEI) 3. They were the Trident volcano in Alaska at 58°N and 155°W and the Vestmannaeyjar volcano (also known as *Surtsey*) south of Iceland at around 63°N and 20°W and. The first was reported to have erupted in April 1963 and its plume reaching 15 km (Decker, 1967). The second remained in in eruption between November 1963 and February 1964, with its plume reaching more than once in November 1963 an altitude around 4.5 km above the tropopause, located approximately at 10.5 km (Thorairinsson, 1965). They were attributed contributing to the replenishing of aerosols in the mid-latitude lower stratosphere, following the increase of the atmospheric turbidity, determined using twilight measurements (Cronin 1971).

Twilight measurements revealed 3 peaks in atmospheric turbidity, between the March 1963 Agung eruption in and the end of 1965 shown in figure 1 from Volz (1970). The first turbidity peak in that figure with the highest magnitude was registered by the end of the 1963, when no lidar measurements were available, but its decaying is seen in the sAOD during the first half of 1964 on our figure 54. The second turbidity peak, having approximately the same magnitude than the third, is located in the last months of 1964, coincident with the second sAOD peak in figure 54. And the third turbidity peak also coincide with the third sAOD peak. Updated information reveal the extension in time of the Vestmannaeyjar, from late 1963 to the middle of 1964 (GVP, 2013a) and the occurrence of two additional eruptions of Trident volcano, the first between October 17 to November 17 1963 and the second in May 31 1964 (GVP, 2013b) all of them with VEI 3. That sustained input of the aerosols in the northern hemisphere stratosphere explains the second and third peaks similar magnitudes in the turbidity, figure 1 in Volz (1970) and in the sAOD in our figure 54.

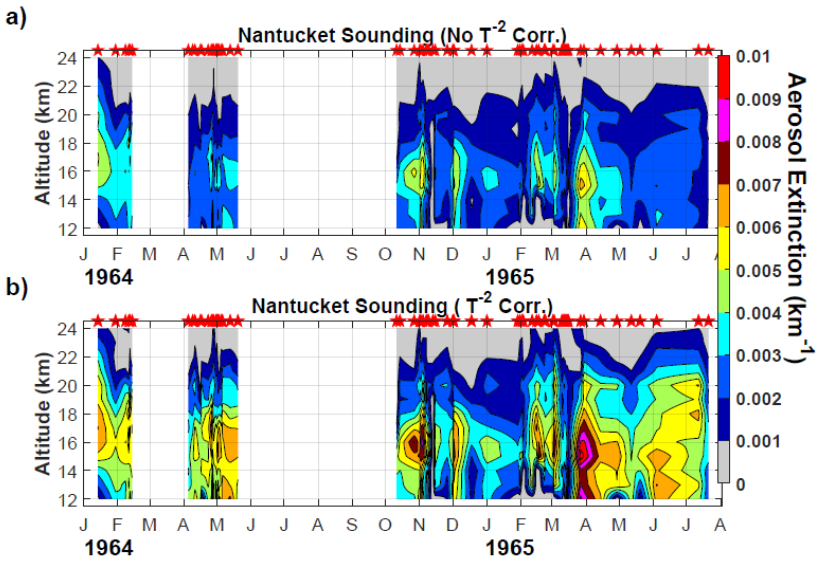

Figure ~~6: Cross-sections~~5: Contours of $\alpha_a(532,z)_*$ for uncorrected and corrected two-way transmittance ($\alpha_a^{Ta}(532,z)$) for Lexington. The red stars indicate the dates the measurements were conducted.

Con formato: Centrado

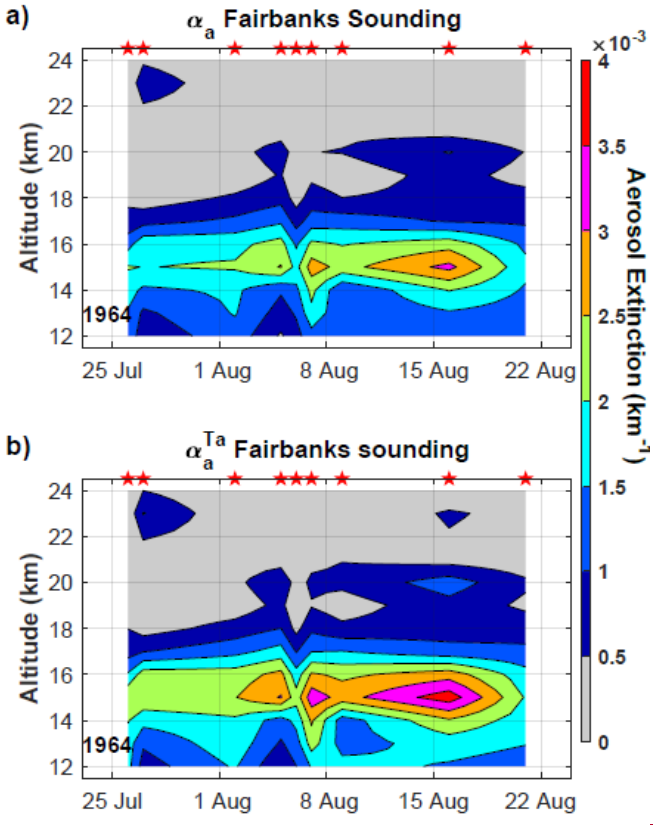

Con formato: Izquierda: 1,9 cm, Derecha: 1,9 cm, Arriba: 2,54 cm, Abajo: 2,54 cm

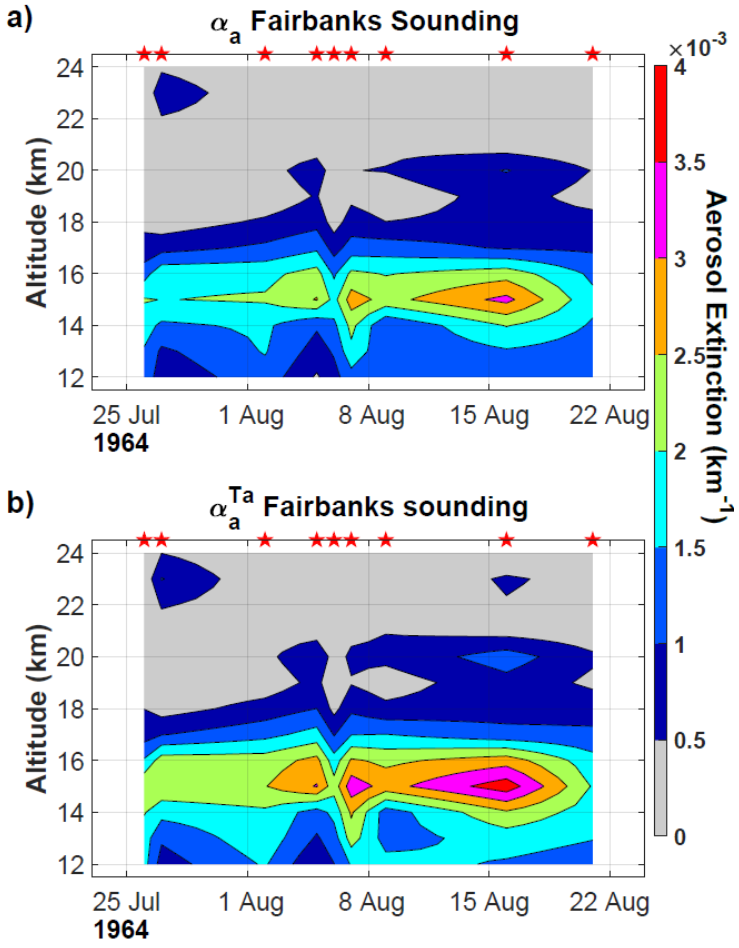

610

Figure ~~7~~6: Cross sections of $\alpha_a(532, z)_*$ for uncorrected and corrected two-way transmittance ($\alpha_a^{Ta}(532, z)$) for Fairbanks. The red stars indicate the dates the measurements were conducted.

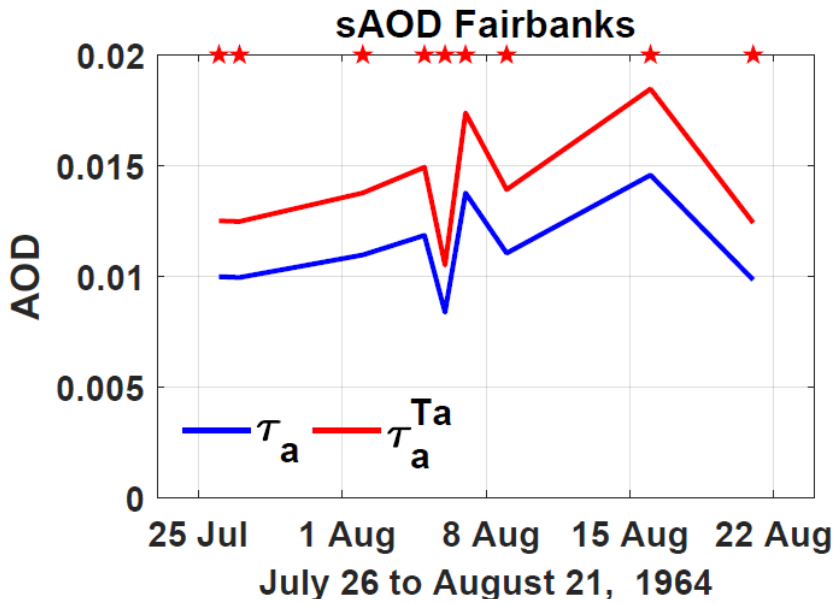

Figure 87: Stratospheric AOD (sAOD) for Fairbank for $\tau_a(532, z)$ and $\tau_a^{Ta}(532, z)$.

615

Con formato: Centrado

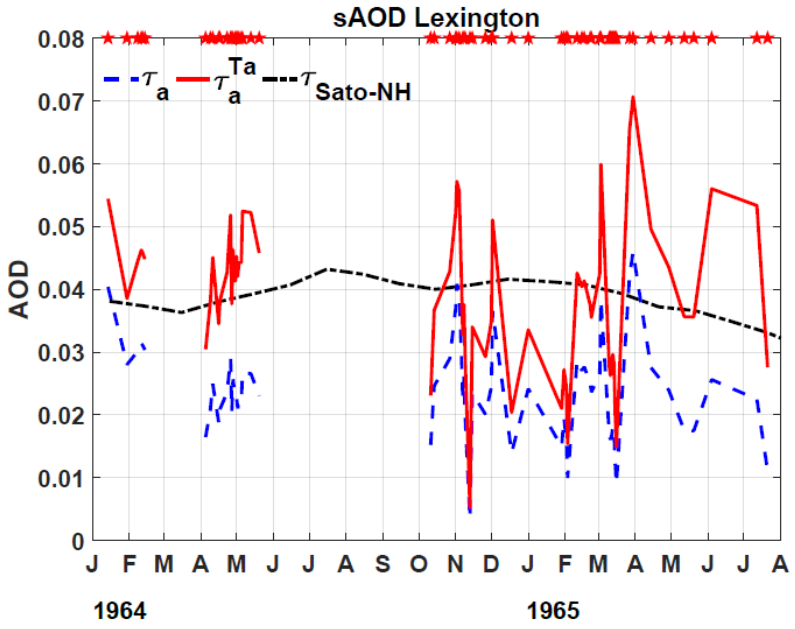

Figure ~~9~~8: Stratospheric AOD (sAOD) for Lexington for $\tau_a(532,z)$ and $\tau_a^{Ta}(532,z)$.

3.3 Relative Errors:

Table ~~5~~4 reports the results for the estimated relative errors in the aerosol extinction with and without the aerosol two-way transmittance correction for both sites. In addition, the relative errors of the backscattering ratio and aerosol backscatter at 694 nm and the aerosol backscatter at 532 nm are reported. The relative errors for $\alpha_a^{Ta} \leq 5 \times 10^{-4}$ km^{-1} were excluded in the statistics.

Note the increases in the mean relative errors from $\left(\frac{\delta SR}{SR}\right)$ to $\left(\frac{\delta \beta_a}{\beta_a}\right)$, 12 % to 48 % at Fairbanks and 13 % to 36 % at Lexington, the higher increases occur during the full processing. It is explained by the factor $\left(\frac{\beta_m}{\beta_a}\right)^2$ in equation (~~2~~18). Because the processing algorithm relies on equation (6) to derive β_a from β_m the squared ratio will be lower than 1 if ~~SR_σ~~ SR < 2, increasing as ~~SR_σ~~ SR decreases and reaching the value $\left(\frac{\beta_m}{\beta_a}\right)^2 = 10^4$ for ~~$SR_\sigma = $~~ SR = 1.01. Only with ~~SR_σ~~ SR => 2 is the

Con formato: Centrado

Con formato: Ancho: 21 cm, Alto: 24 cm

ratio is lower than 1, which in the case of Fairbanks happens at one level on one day. In the case of Lexington, 10% of the $\mathbf{SR_o}$ are higher than 2. In other words

In table ~~5~~4, the second ~~high~~highest increase in the mean relative error ~~happened~~occurs in the calculation of $\left(\frac{\delta\alpha_a^{Ta}}{\alpha_a^{Ta}}\right)$ from $\left(\frac{\delta\alpha_a}{\alpha_a}\right)$. At Fairbanks the increase is 7%, from 54% to 61~~%. At~~% and at Lexington the increase is 20% from 44% to 64%. The error is associated with the magnitudes of the relative errors from $\left(\frac{\delta T_a}{T_a}\right)$, conducted at this step ~~by~~for the reasons explained above. At Fairbanks the mean value of $\left(\frac{\delta T_a}{T_a}\right)$ is 8% while 44% at Lexington, associated ~~to~~with the expression $\delta\tau_a = 0.5\ \tau_a$. It should be taken into account that the total AOD at both sites are dominated by the magnitude of the tropospheric AOD, which is higher at Lexington.

Table ~~5~~4: Relative error estimates of the backscattering ratio, aerosol backscatter at 694 nm and 532 nm, aerosol extinction with and without correction for aerosol two-way transmittance at 532 nm for Lexington and Fairbanks. Errors for $\alpha_a^{Ta} \leq 5 \times 10^{-4}$ km^{-1} were not included in the statistics. All errors are %.

FAIRBANKS							LEXINGTON					
	694 nm		532 nm				694 nm		532 nm			
	$\left(\frac{\delta SR}{SR}\right)$	$\left(\frac{\delta\beta_a}{\beta_a}\right)$	$\left(\frac{\delta\beta_a}{\beta_a}\right)$	$\left(\frac{\delta\alpha_a}{\alpha_a}\right)$	$\left(\frac{\delta T_a}{T_a}\right)$	$\left(\frac{\delta\alpha_a^{Ta}}{\alpha_a^{Ta}}\right)$	$\left(\frac{\delta SR}{SR}\right)$	$\left(\frac{\delta\beta_a}{\beta_a}\right)$	$\left(\frac{\delta\beta_a}{\beta_a}\right)$	$\left(\frac{\delta\alpha_a}{\alpha_a}\right)$	$\left(\frac{\delta T_a}{T_a}\right)$	$\left(\frac{\delta\alpha_a^{Ta}}{\alpha_a^{Ta}}\right)$
Mean	12%	48%	49%	54%	8%	61%	13%	36%	38%	44%	21	64%
Maximum	13%	120	121	122	8%	125%	16%	151	151	152	42	162%
Minimum	11%	24%	26%	31%	7%	42%	11%	18%	20%	27%	9%	43%

The ~~vertical distributions~~time vs. altitude contours of the $\left(\frac{\delta\alpha_a^{Ta}}{\alpha_a^{Ta}}\right)$ ~~realtive~~relative errors ~~on consecutive measurements~~and of the $\alpha_a^{Ta}(z,n)$ are shown in figures ~~10~~9 and ~~11~~10 for Lexington and Fairbanks respectively. ~~Panels a) in both figures are the cross-sections of the $\left(\frac{\delta\alpha_a^{Ta}}{\alpha_a^{Ta}}\right)$ relative errors and panels b) are the cross-sections of the $\alpha_a^{Ta}(z,n)$, where n is the consecutive number order of the measurements in each one of the datasets. We selected this variable to provide a compact view of the magnitudes of the $\left(\frac{\delta\alpha_a^{Ta}}{\alpha_a^{Ta}}\right)$ relative errors and α_a^{Ta}. As expected at both sites the~~The regions with maximum magnitudes of α_a^{Ta} at both sites are associated with the lower relative errors~~. In figure 10 note that at~~ as expected. At Lexington, for $\alpha_a^{Ta} > 8 \times 10^{-3}$ km^{-1} the relative errors ~~has a magnitude equal or lower than~~are <= 30%. It is also evident that relative errors equal or lower than 50% dominate both in time and altitude. In the case of Fairbanks, ~~figure 11, for~~ $\alpha_a^{Ta} > 2 \times 10^{-3}$ km^{-1} the relative ~~error has a magnitude equal or lower than~~errors are <= 40%.

~~Considering the magnitudes of the~~ The relative errors ~~for~~of α_a^{Ta}, in table ~~5 it is evident that the~~4, produce τ_a^{Ta} relative errors ~~are~~ above 100%. Those estimated values of the relative errors for τ_a^{Ta} together with the ones in table ~~5 show high~~

Tabla con formato

Con formato: Fuente: Negrita

~~magnitudes compared with~~4 are substantially larger than other sets of volcanically perturbed stratospheric aerosols lidar measurements.

~~As explained above, the highest~~The high error ~~introduced~~magnitudes in the $\left(\frac{\delta\beta_a}{\beta_a}\right)$ at 694 nm estimation could be reduced ~~if~~in case the $\mathbf{SR_o}$ ~~have higher~~ values increase. In several of the 75 $\mathbf{SR_o}$ profiles a renormalization processing could increase ~~its~~$\mathbf{SR_0}$ magnitude. ~~That~~This is ~~possible, because~~reasonable since the normalization ~~procedure applied, considered that above 24~~altitude range (no aerosol present) was 25 to 30 km ~~no aerosols were~~, where there certainly would be some aerosol present. Inspection of the plots of $\mathbf{SR_o}$ vs altitude in figures 14, 15 and 16 in **G-66** shows the presence of aerosols between 25 and 30 km ~~and~~. And in some of the ~~cases at all of those levels~~ profiles $\mathbf{SR_o}$ ~~magnitude~~ is above 1~~, the value representing~~ at all levels (1.0 indicates no ~~aerosols~~aerosol). In addition, ~~what will definitely increase the magnitude of $\mathbf{SR_o}$, will be the introcution~~the introdution of the two-way transmittance correction in the processing ~~generation~~of $\mathbf{SR_o}$, will increase $\mathbf{SR_o}$ from the raw returned lidar signal.

~~In the search for~~ Options are available to find the raw lidar data ~~several options are available. Searching~~to conduct the reproccesing described above. These include searching for the filmed images of the oscilloscopes used as registers and/or the original punched cards (probably transferred to tapes) both reported in **G-66**. ~~The~~A last resort would be the digitalization of the $\mathbf{SR_o}$ from the figures cited above. ~~Then the~~The original signal profiles could then be reconstructed inverting the normalization procedure applied to produce the $\mathbf{SR_o}$ profiles.

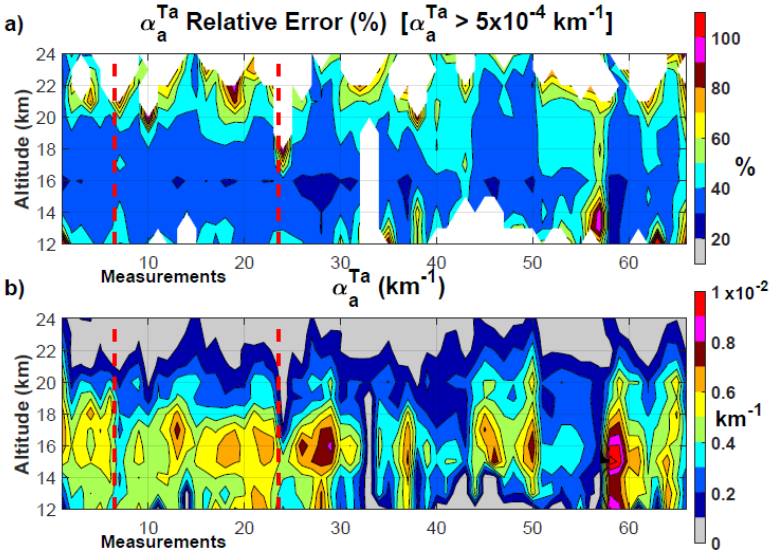

Con formato: Punto de tabulación: 9,25 cm, Izquierda

Con formato: Centrado

Figure ~~10: Cross-section~~9: Panel a) Contour of Relative Error estimates for Lexington~~, panel a).~~. Panel b) ~~Cross-section~~Contour of the consecutive measurements. Note the two data gap periods greater than 1 month: March, and July to September both in 1964. They are identified with vertical dotted red lines at the 7 and 23 measurements. In top panel the areas in white in the Relative Error ~~cross-section~~contour represent relative errors for $\alpha_a^{Ta} \leq 5 \times 10^{-4}$ km^{-1}. They were not included in the statistics in Table ~~5~~4.

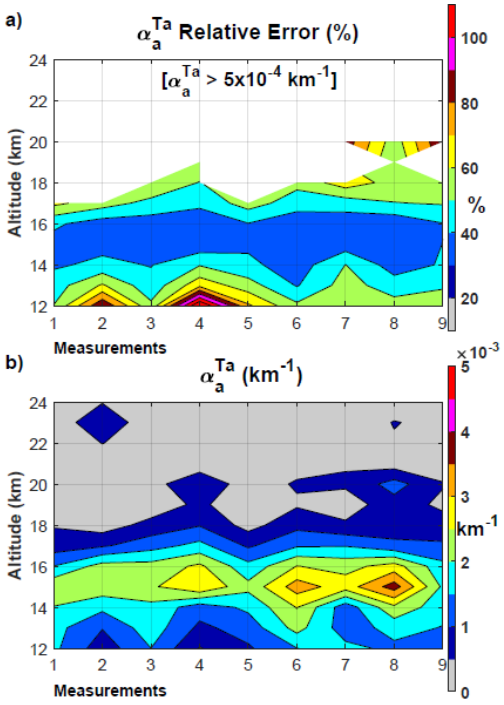

Figure ~~11~~10: Idem figure ~~10~~9 but for Fairbanks.

3.4 Attribution of the 1963 Agung aerosol cloud within the Lexington lidar dataset:

In this section, we seek to understand whether some of the sAOD variations observed by the Lexington lidar may originate from sources other than the March 1963 Agung eruption (such as the two stratosphere-injecting 1963 VEI3 discussed in

Con formato: Centrado

section 3.2: Trident, Alaska and Vestmannaeyjar, Iceland). Specifically, we compare the Lexington extinction dataset to four different model-based volcanic forcing datasets for the Agung aerosol cloud. Three of the four Agung forcing datasets are from two different interactive stratospheric aerosol models: two different SO_2 emissions scenarios from the UM-UKCA model (Dhomse et al., 2020) and a third simulation from the 2D-AER model (Arfeuille et al. 2014), as applied within the CMIP6 volcanic aerosol dataset (Luo et al., 2016). The fourth ~~simulations~~simulation is from an ~~idealised~~idealized model representation of the Agung cloud, based on a simple parameterization for the progression of the tropical reservoir of volcanic aerosol, and its dispersion to mid-latitudes (Ammann et al., 2003), used to represent historical volcanic forcings in some CMIP5 climate model historical integrations (see Driscoll et al., 2012).

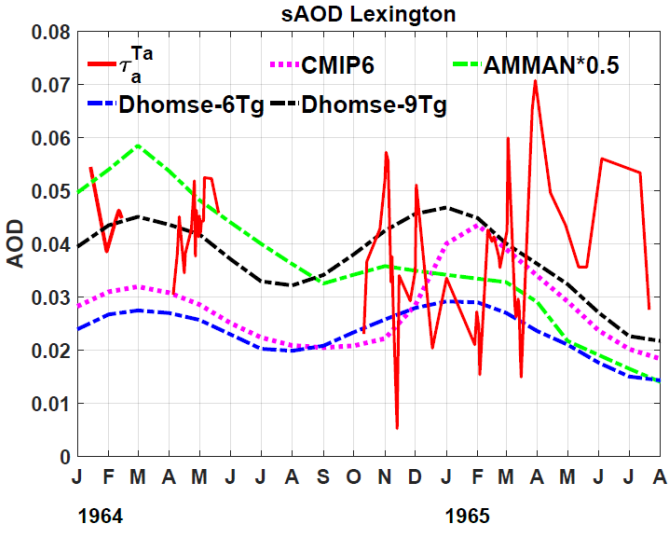

Figure ~~12~~11: Model representations of the Agung aerosol cloud sAOD compared to the Lexington dataset.

The progression of volcanic aerosol clouds from major tropical eruptions reaching the stratosphere was established by Dyer et al. (1970; 1974~~) from analysing~~). They synthesized the extensive ~~synthesis~~set of observations on the Agung aerosol cloud (Dyer and Hicks, 1968), and ~~from knowledge derived from~~used the analyses of the global dispersion of radionuclides from Pacific thermonuclear tests in the 1950s (e.g. Machta and List, 1959). The continual slow upwelling circulation in the tropics, and the sub-tropical barrier at the edge of the tropical pipe, combine to cause the long-lived tropical stratospheric reservoir (Dyer, 1974; Grant et al., 1996) which is the reason why tropical eruptions have such prolonged radiative cooling compared to mid-latitude eruptions. The Brewer -Dobson circulation (Brewer, 1949; Dobson, 1956) has a strong seasonal cycle,

Con formato: Centrado

Con formato: Normal, Izquierda, Sangría: Izquierda: 0 cm, Derecha: 0 cm, Interlineado: sencillo

transporting air preferentially towards the winter pole, causing an increasing mid-latitude sAOD trend during autumn and a decreasing mid-latitude sAOD trend during spring (in both hemispheres). Each of the model lines in ~~Figure 12~~figure 11 show this circulation-driven seasonal variation in sAOD, with the transport of the Agung aerosol remaining in the tropical reservoir predicted to increase during October and November, reaching a peak in January to March in both 1964 and 1965. The model predicted variations are consistent with the initial observed sAOD values of 0.04-0.05 in January and February 1964 being higher than most of the 0.01-0.04 sAOD values observed in October and November 1964, and the expected variations from the models suggest the suddenly higher sAOD values ~0.05 may be from a different source than Agung. However, whereas sAOD values would be expected to increase going into winter, the December January and February sAOD at Lexington are mostly lower than during the autumn, which indicates an additional source of stratospheric aerosol may have continued to add to the Agung cloud sAOD throughout the autumn of 1964. Furthermore, the 1965 Lexington observations show a continuing increase in sAOD into the springtime, whereas the models predict the sAOD from Agung would have reduced by a factor of 2 during the first 6 months of 1965. The analysis suggests another source of sAOD influential during this period (either the two VEI3 volcanic eruptions in 1963/4 or some other source of material into the stratosphere) must have caused the observed increase in stratospheric AOD during 1965, with a potentially substantial influence also during autumn 1964.

Figure ~~13~~12 compares the vertical structure of the 9Tg representation of the Agung aerosol cloud from Dhomse et al. (2020) at 42N, compared to the Lexington observations, confirming that these model simulations capture the altitude of the cloud during the early period of the measurements (January to May 1964). However, although the magnitude of the simulated aerosol extinction compared well to the original Lexington dataset (Dhomse et al., 2020), with the two-way transmittance corrections applied here, the 9Tg simulation is low-biased compared to the lidar measurements, even in this earlier period, suggesting ~~a with~~ the 12Tg UM-UKCA simulation (not shown) would likely ~~to~~ compare better ~~(not shown).~~ None of the 4 model-generated Agung forcing datasets can explain the observed increase in extinction during Jan to July 1965~~, with the~~. The sudden peaks in April and June 1965 ~~having a~~have quite a different vertical structure compared to the early 1964 measurements, the sAOD in 1965 having a substantial component from the altitude range 18-20km. This vertical profile analysis again suggests the episodic sAOD enhancements in spring 1965 were from a different source than the 1964 measurements~~, the altitude of the peak extinction in that first year of the dataset broadly consistent with the UM-UKCA simulations of the Agung cloud~~.

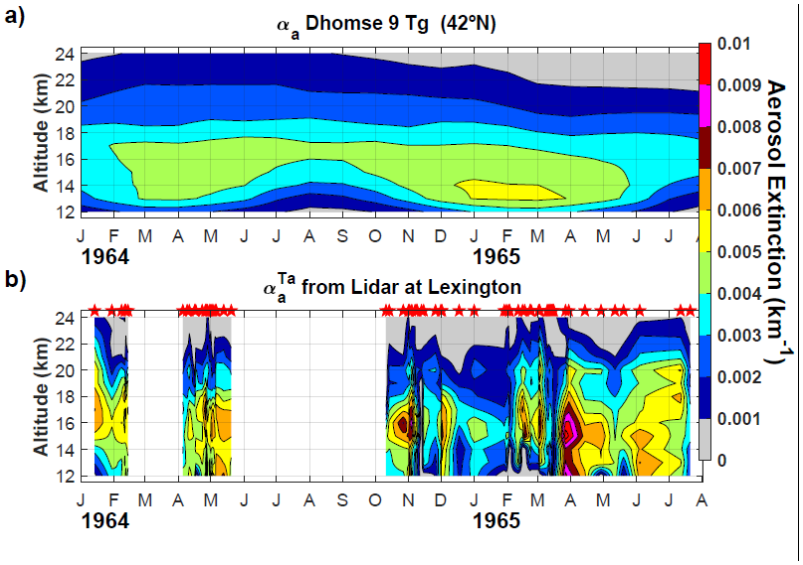

Figure ~~13: Cross sections~~12: Contours of $\alpha_a(532,z)_*$ from Dhomse et al., (2020) at 42 °N and corrected the two-way transmittance $\alpha_a^{Ta}(532,z)$ from lidar for Lexington.

Con formato: Centrado

Summary:

We ~~report completing~~completed the processing of the first set of volcanic stratospheric aerosol lidar profiles~~,~~ from the 1963 Mt. Agung eruption. The results show the high level of variability of the stratospheric aerosol extinction for Lexington between January 1964 and July 1965 that is mainly attributed to the 1963 Mt. Agung eruption. At Lexington the highest aerosol extinction values and aerosol optical depths are 1.1 x 10^{-2} km^{-1} and 0.076 respectively and were ~~registered~~observed by the end of March 1965, almost at the end of the year and a half long record. Based on contemporary and updated reports of additional volcanic eruptions in the northern hemisphere between1963 and 1965 we found a probable explanation to the apparent contradictory temporal trend of the sAOD magnitudes. Further research, combining observational data and modelling should be conducted to elucidate the individual contribution from each of those eruptions to the stratospheric aerosol layer at this location of the northern hemisphere.

The level of the relative errors are unusually high considering that under high loads of volcanic aerosols in the stratosphere, the signal to noise ratio is high in the returned lidar signal. The analysis of the contributions of the variables along the different steps of the processing algorithm, ~~allowed identifying~~identified the two main sources of error. The main one, accounting for a little more than 30 % of the relative error is associated with the division of the molecular backscatter by the aerosol backscatter, directly linked to low magnitudes of the backscattering ratio. Those low magnitudes are produced by two factors: the first is the lack of two-way transmittance corrections in the backscattering ratio calculation from the raw squared distance-corrected signal. The second is that the normalization ~~method conducted in the region~~altitudes, considered to be empty of aerosols, ~~when in many profiles the signal plots reveal its presence~~were too low and actually did contain aerosol. We suggested alternatives to search for the original signal profile records or to reconstruct the original signal profiles from the plotted backscattering ratio records, including the normalization region from 25 to 30 km. ~~The~~Future search for original records should ~~include looking for~~take into account also the ~~at least~~ 25 missing ~~profiles~~files from the ~~total~~more of ~~at least~~ 100 referred by Fiocco ~~mentions~~.

In general the results reported should be considered as the first estimates. We report the comparison of the aerosol extinction values and aerosol optical depths we calculated with information available up to the present, showing reasonable results. Improvements in the two factors cited above lead to an increase in magnitude of the aerosol extinction and optical depth in several of the profiles.

We have also compared the Lexington sAOD ~~timeseries~~time series to 4 different model representations of the 1963 Agung aerosol cloud, and illustrate how the model predictions suggest the sAOD above Lexington from Agung must have decreased from January to July 1965, whereas the 1965 lidar observations show a clear increase in sAOD through the spring into summer. ~~Comparison of the vertical structure of the 1965 measurements to the~~The UM-UKCA Agung aerosol simulations show the Agung cloud descending to lower altitude in 1965 than in 1964~~, whereas~~. Whereas the lidar measurements show more sudden aerosol extinction enhancements, reaching up to 20km in altitude during 1965. Contemporary records of two VEI-3 high latitude eruptions (in Alaska and Iceland) suggest their volcanic clouds reached the stratosphere in both cases,

and model comparisons strengthen the attribution of the January to July 1965 $sAOD_{550}$ increase to a source other than the 1963 Agung eruption.

The datasets of the original rescued backscattering ratios and the calculated aerosol backscatter (both at 694 and 532 nm) and the aerosol extinction at 532 nm (both corrected and uncorrected for two-way aerosols transmittances) at Lexington are available at https://doi.pangaea.de/10.1594/PANGAEA.922105 (*Dataset in Review*) (Antuña-Marrero et al., 2020a).

Acknowledgements:

To the memory of Dr. Giorgio Fiocco, Dr. Gerald W. Grams, for their pioneering research on lidar measurements in particular the stratospheric aerosols from the Mt. Agung 1963 eruption. We have included them as co-authors as an homage to their pioneering work. We acknowledge funding from the U.K. National Centre for Atmospheric Science (NCAS) for Dr. Graham Mann via the NERC multi-centre Long-Term Science programme on the North Atlantic climate system (ACSIS). We also acknowledge support from the Copernicus Atmospheric Monitoring Service (CAMS), one of 6 services that together form Copernicus, the EU's Earth observation programme. The global aerosol development tender within CAMS (CAMS43) funded Juan-Carlos Antuna's 1-month visit to Leeds in March 2019, and 50% co-funded the PhD studentship of Sarah Shallcross, with matched funding from the Institute for Climate and Atmospheric Science, School of Earth and Environment, Univ. Leeds. Dr. Sandip Dhomse and Dr. Graham Mann received funding via the NERC highlight topic consortium project SMURPHS ("Securing Multidisciplinary UndeRstanding and Prediction of Hiatus and Surge periods", NERC grant NE/N006038/1. The UM-UKCA simulations were performed on the UK ARCHER national supercomputing service with data analysis and storage within the UK collaborative JASMIN data facility. We acknowledge the contribution from Brent Holben for providing the information about the contemporary turbidity measurements. Also the PI's of the AERONET sites for their valuable datasets and Norman T. O'Neill from CARTEL for his contribution with relevant articles. Thanks to Terry Deshler and Horst Jäger for contributing the magnitudes of relative errors for the backscatter to extinction conversion coefficients and the wavelengths exponents. Their comments and suggestions were also very valuable ~~too~~. JCAM recognizes the support from the Optics Atmospheric Group, Department of Theoretical, Atomic and Optical Physics, University of Valladolid Spain.

Data availability:

The data reported in this article is available at https://doi.pangaea.de/10.1594/PANGAEA.922105 (*Dataset in Review*) (Antuña-Marrero et al., 2020a).

References:

~~AERONET, 2020, Aerosol Robotic Network, http://aeronet.gsfc.nasa.gov/~~

Con formato: Inglés (Estados Unidos)

Con formato: Inglés (Estados Unidos)

Ammann, C. M., Meehl, G., Washington, W. M. and Zender, C. S, A monthly and latitudinally varying volcanic forcing dataset in simulations of 20th century climate, Geophys. Res. Lett., vol. 30, no. 12, doi:10.1029/2003GL016875, 2003.

Ångstrom, A., On the atmospheric transmission of Sun radiation and on dust in the air, *Geogr. Ann.*, **12**, 130-159, 1929.

Antuña-Marrero, J.-C., Mann, G. W., Barnes, J., Rodríguez-Vega, A., Shalcross, S., Dhomse, S., Fiocco, G., Grams, G. W., Mt Agung 1963 attributed, stratospheric aerosols lidar dataset from Lexington, MA, and Fairbanks, AK. PANGAEA, https://doi.pangaea.de/10.1594/PANGAEA.922105, 2020a.

Antuña-Marrero, J. C., Mann, G. W. , Keckhut, P., S. Avdyushin, B. Nardi and and L. W. Thomason, Ship-borne lidar measurements showing the progression of the tropical reservoir of volcanic aerosol after the June 1991 Pinatubo eruption. , *Earth Syst. Sci. Data,* (*Under Discussion*), https://doi.org/10.5194/essd-2020-81, 2020b.

Arfeuille, F., Weisenstein, D., Mack, H., Rozanov, E., Peter, T. and Broennimann, S. Volcanic forcing for climate modeling: a new microphysics-based data set covering years 1600–present, Clim. Past, 359-375, 2014.

Bauer, S. E., Tsigaridis, K., Faluvegi, G., Kelley, M., Lo, K. K., Miller, R. L., et al, Historical (1850-2014) aerosol evolution and role on climate forcing using the GISS ModelE2.1 contribution to CMIP6. *Journal of Advances in Modeling Earth Systems*, **12**, e2019MS001978. https://doi.org/10.1029/2019MS001978, 2020.

Bodhaine B. A., N. B. Wood, E. G. Dutton, and J. R. Slusser: On Rayleigh optical depth calculations, *J. Atmos. Ocean Technol.*, **16**, 1854-1861, 1999.

Brewer, A. W.: Evidence for a world circulation provided by the measurements of helium and water vapour in the stratosphere, *Q. J. Roy. Meteorol. Soc.*, vol. 75, 351-363, 1949.

Clemesha, B. R., Kent, G. S. and Wright, R. W. H., Laser probing of the lower atmosphere, *Nature*, **210**, 184.

Clemesha, B. R., Comments on a Paper by A. I. Dyer, Anisotropic Diffusion Coefficients and the Global Spread of Volcanic Dust, *J. Geophys. Res.*, **76**, 755-756, 1971

COESA, Committee on Extension to the Standard Atmosphere, U. S. Standard Atmosphere Supplements 1966, U.S. Government Printing Office, Washington, D.C., 1967.

CollisCollins, R. T. H., and P. B. Russell: Lidar measurement of particles and gases by elastic backscattering and differential absorption, Laser Monitoring of the Atmosphere, E. D. Hinkley (editor), (Springer-Verlag, 1976), Chapter 4, 1976

Cronin, J. F., Recent Volcanism and the Stratosphere, *Science*, **172**, 847-849, 1971.

Decker, R.W., 1967. Investigations at active volcanoes. *Trans. Am. Geophys. Union*, **48**: 639--647.

Deshler, T., A review of global stratospheric aerosol: Measurements, importance, life cycle and local stratospheric aerosol, *Atmos. Res.*, **90**, 223-232, 2008.

Deirmendjian, D., Note on Laser Detection of Atmospheric Dust Layers, *J. Geophys. Res.*, **70**, 743 – 745, 1965

Deirmendjian, D., Global Turbidity Studies. I. Volcanic Dust Effects - A Critical Survey, Rand Corp., Report R-886-ARPA, 74 pp., https://apps.dtic.mil/dtic/tr/fulltext/u2/736686.pdf, 1971

Dhomse, S. S., Mann, G. W., Antuña Marrero, J. C., Shallcross, S. E., Chipperfield, M. P., Carslaw, K. S., Marshall, L., Abraham, N. L., and Johnson, C. E.: Evaluating the simulated radiative forcings, aerosol properties, and stratospheric warmings from the 1963 Mt Agung, 1982 El Chichón, and 1991 Mt Pinatubo volcanic aerosol clouds, *Atmos. Chem. Phys. Discuss.*, https://doi.org/10.5194/acp-2020-344 , in review, 2020. *Atmospheric Chemistry and Physics*, *20*(21), pp.13627-13654, 2020

Dobson, G. M. B. Origin and distribution of the polyatomic molecules in the atmosphere, *Proc Roy. Soc. London. A*, **236**,. 1205, 187-193, 1956.

Driscoll, S., Bozzo, A., Gray, L. J., Robock, A. and Stenchikov, G., Coupled Model Intercomparison Project 5 (CMIP5) simulations of climate following volcanic eruptions, *J. Geophys. Res.*, **117**, doi:10.1029/2012JD017607, 2012.

Durre, Imke, Xungang, Yin, Vose, Russell S., Applequist, Scott, Arnfield, Jeff. Integrated Global Radiosonde Archive (IGRA), Version 2. [Individual soundings]. NOAA National Centers for Environmental Information. DOI:10.7289/V5X63K0Q [Accesed: April,3 2020], 2016.

Dyer, A. J. and Hicks, B. B.: Global spread of volcanic dust from the Bali eruption of 1963, *Q. J. Roy. Meteorol. Soc.*, **94**, 545– 554, https://doi.org/10.1002/qj.49709440209, 1968.

Dyer, A. J.: Anisotropic diffusion coefficients and the global spread of volcanic dust, *J. Geophys. Res.*, **75**, 15, 3007-3012, 1970

Dyer, A. J., Reply, *J. Geophys. Res.*, **76**, 2898, 1971a.

Dyer, A. J., Volcanic dust in the Northern Hemisphere, *J. Geophys. Res.*, **76**, 757, 1971b.

Dyer, A. J., The effect of volcanic eruptions on global turbidity and an attempt to detect long-term trends due to man, *Q. J. Roy. Meteorol. Soc.*, **100**, 563-571, 1974.

Elterman, L., Aerosol MeasurementsAtmospheric attenuation model, 1964, in the Troposphereultraviolet, visible, and infrared regions for altitudes to 50 km, Report AFCRL-64-740, AFCRL, 1964.

Elterman, L. and Campbell, A. B., Atmospheric aerosol observations with searchlight probing, *J. Atmospheric Sci.* **21**, 457, 1964.

Eyring, V., Bony, S., Meehl, G. A., Senior, C. A., Stratosphere, *Appl. Opt.*, **5**, 1769-1776, 1966Stevens, B., Stouffer, R. J., and Taylor, K. E.: Overview of the Coupled Model Intercomparison Project Phase 6 (CMIP6) experimental design and organization, *Geosci. Model Dev.*, **9**, 1937-1958, https://doi.org/10.5194/gmd-9-1937-2016, 2016.

Fiocco, G., Smullin, L., Detection of scattering layers in the upper atmosphere (60–140 km) by optical radar. *Nature* **199**, 1275–1276. https://doi.org/10.1038/1991275a0 , 1963.

Fiocco, G., and G. Colombo, 1964: Optical radar results and meteoric fragmentation. *J. Geophys. Res.*, **69**, 1795–1803, https://doi.org/10.1029/JZ069i009p01795 , 1964.

Fiocco, G., and G. Grams, Observations of the aerosol layer at 20 km by optical radar. *J. Atmos. Sci.*, **21**, 323–324, https://doi.org/10.1175/1520-0469(1964)021<0323:OOTALA>2.0.CO;2 , 1964.

Con formato: Color de fuente: Color personalizado(RGB(34;34;34)), Inglés (Reino Unido), Diseño: Claro (Blanco)

Fiocco, G., Sensing of Meteorological Variables by Laser Probe. Semi-annual report, 1 Feb. - 31 Jul. 1966, NASA-Grant-22-009-131, CR-77909, 1966a.

Fiocco, G., Laser Probing of the Atmosphere. Semi-annual status report, March 1966, NASA-Grant-10-007-028, CR-74730, 1966b.

~~Flowers, E. C., R. A. McCormick, and K. R. Kurfis, Atmospheric turbidity over the United States, 1961-1966, *J. Appl. Meteor.*, **8**, 955-962, 1969.~~

~~Freund, J., Aerosol optical depth in the Canadian arctic, *Atmosphere-Ocean*, **21**:2, 158-167, DOI: 10.1080/07055900.1983.9649162, 1983.~~

~~Grams, G., Optical radar studies of stratospheric aerosols. PhD Thesis, 121 pp., https://dspace.mit.edu/bitstream/handle/1721.1/13502/25776466-MIT.pdf , 1966.~~

~~Grams, G ., and G. Fiocco, Stratospheric aerosol layer during 1964 and 1965, *J. Geophys. Res.*, **72**, 3523-3542, 1967.~~

Global Volcanism Program, 2013a. Vestmannaeyjar (372010) in Volcanoes of the World, v. 4.9.0 (04 Jun 2020). Venzke, E (ed.). Smithsonian Institution. Downloaded 16 Jul 2020 (https://volcano.si.edu/volcano.cfm?vn=372010). https://doi.org/10.5479/si.GVP.VOTW4-2013, 2013.

~~Grant, W. B., Browell, E. V., Long, C. S., Stowe, L. L., Grainger, R. G and Lambert, A.: Use of volcanic aerosols to study the tropical stratospheric reservoir, *J. Geophys. Res.*, 101 (D2), 3973-3988, 1996.~~

Global Volcanism Program, 2013b. Trident (312160) in Volcanoes of the World, v. 4.9.0 (04 Jun 2020). Venzke, E (ed.). Smithsonian Institution. Downloaded 16 Jul 2020 (https://volcano.si.edu/volcano.cfm?vn=312160). https://doi.org/10.5479/si.GVP.VOTW4-2013, 2013.

Grams, G., Optical radar studies of stratospheric aerosols. PhD Thesis, 121 pp., https://dspace.mit.edu/bitstream/handle/1721.1/13502/25776466-MIT.pdf , 1966.

Grams, G ., and G. Fiocco, Stratospheric aerosol layer during 1964 and 1965, *J. Geophys. Res.*, **72**, 3523-3542, 1967.

Grant, W. B., Browell, E. V., Long, C. S., Stowe, L. L., Grainger, R. G and Lambert, A.: Use of volcanic aerosols to study the tropical stratospheric reservoir, *J. Geophys. Res.*, 101 (D2), 3973-3988, 1996.

Hansen, J. E., Wang, W.-C. and Lacis, A. A.: Mount Agung eruption provides test of global climatic perturbation, Science, 199, 1065-1068, 1978.

Hering, W. S., and T. R. Borden, Jr., Ozonesonde Observations over North America, 4, Environmental Research Papers, No. 279, Air Force Cambridge Research Laboratories, Report AFCRL-64-30(IV), 1967.

Hostetler, C. A., Z. Liu, J. Regan, M. Vaughan, D. Winker, M. Osborn, W. H. Hunt, K. A. Powell, and C. Trepte, CALIOP Algorithm Theoretical Basis Document (ATBD): Calibration and level 1 data products, Doc. PC-SCI-201, NASA Langley Res. Cent., Hampton, Va., 2006. (Available at https://www-calipso.larc.nasa.gov/resources/pdfs/PC-SCI-201v1.0.pdf)

Husar, R. B., J. M. Holloway, D. E. Patterson, W. E. Wilson, Spatial and temporal pattern of eastern U.S. haziness: A summary, *Atm. Env.* **15**, 10–11, 1919-1928, 1981.

Con formato: Fuente: Sin Cursiva

Con formato: Hipervínculo, Inglés (Reino Unido)

Con formato: Hipervínculo, Inglés (Reino Unido)

Con formato: Francés (Francia)

Con formato: Hipervínculo, Inglés (Reino Unido)

Con formato: Francés (Francia)

Con formato: Fuente: Sin Cursiva

Jäger, H., and T. Deshler, Lidar backscatter to extinction, mass and area conversions for stratospheric aerosols based on midlatitude balloon-borne size distribution measurements, *Geophys. Res. Lett.*, 29(19), 1929, https://doi.org/10.1029/2002GL015609 , 2002

Jäger, H., and T. Deshler, Correction to Lidar backscatter to extinction, mass and area conversions for stratospheric aerosols based on midlatitude balloonborne size distribution measurements, *Geophys. Res. Lett.*, **30**(7), 1382, https://doi.org/10.1029/2003GL017189 , 2003.

Klett, J. D., Stable Analytical Inversion Solution for Processing Lidar Returns, *Appl. Opt.* **20**, 211, 1981.

Klett, J. D., Lidar inversion with variable backscatter/extinction ratios, *Appl. Opt.* **24,** 1638, 1985.

Kovalev, V. A., Solutions in lidar profiling of the atmosphere. John Wiley & Sons, Inc., Hoboken, New Jersey, 544 pp, ISBN 978-1-118-96328-9, 2015

.

Luo, B., Stratospheric aerosol data for use in CMIP6 models – data description, ftp://iacftp.ethz.ch/pub_read/luo/CMIP6/Readme_Data_Description.pdf, 2016.

Machta, L. and List, R. Analysis of stratospheric Strontium measurements, *J. Geophys. Res.*, 64, 9, 1267-1276, 1959.

McCormick, M. P., and R. E. Veiga, SAGE II measurements of early Pinatubo aerosols, *Geophys. Res. Lett.*, **19**, 155-158, 1992.

Niemeier, U., Timmreck, C., and Krüger, K.: Revisiting the Agung 1963 volcanic forcing – impact of one or two eruptions, *Atmos. Chem. Phys*., **19**, 10379–10390, https://doi.org/10.5194/acp-19-10379-2019, 2019.

Orphal, J., et al., Absorption cross-sections of ozone in the ultraviolet and visible spectral regions: Status report 2015. *Journal of Molecular Spectroscopy,* **327**, 105–121, 2016.

Robock, A.: Volcanic eruptions and climate, *Rev. Geophys.,* **38**,191–219, https://doi.org/10.1029/1998RG000054, 2000.

Rosen, J. M., The Vertical Distribution of Dust to 30km, J. Geophys. Res., 69 (21), 4673-4767, 1964.

Rosen, J. M., Simultaneous Dust and Ozone Soundings over North and Central America, J. Geophys. Res., vol. 73, no. 2, 479-486, 1968.

Russell, P. B., T. J. Swissler, and M. P. McCormick, Methodology for error analysis and simulation of lidar aerosol measurements, *App. Opt.*, **18**, 3783-3797, 1979.

Sato, M., Hansen, J. E., McCormick, M. P., and Pollack, J. B., Stratospheric aerosol optical depths, *J. Geophys. Res.*, **98**, 22987, https://doi.org/10.1029/93JD02553, 1993.

~~Serdyuchenko, A., Gorshelev, V., Weber, M., Chehade, W., and Burrows, J. P.: High spectral resolution ozone absorption crosssections – Part 2: Temperature dependence, *Atmos. Meas. Tech.*, **7**, 625–636, doi:10.5194/amt-7-625-2014, 2014.~~

~~Shaw, G. E., J. A. Reagan and B. M. Herman, 1973: Investigations of atmospheric extinction using direct solar radiation measure ments made with a multiple wavelength photometer. *J. Appl. Meteor.*, **12**, 374-380.~~

~~Shaw, G. E., Atmospheric Turbidity in the Polar Regions, *Journal of Applied Meteorology*, **21**, 8, pp. 1080-1088, 1982.~~

Smullin, L. D., and Fiocco, G., Optical Echoes from the Moon, *Nature,* **194**, 1267, https://doi.org/10.1038/1941267a0 , 1962.

Con formato: Hipervínculo, Inglés (Reino Unido)

Con formato: Hipervínculo, Inglés (Reino Unido)

SSiRC, Activity – Data Rescue http://www.sparc-ssirc.org/data/datarescueactivity.html (last access: 19 May 2020), 2020.

Stothers, R. B.: Major optical depth perturbations to the stratosphere from volcanic eruptions: Stellar extinction period, 1961–1978, *J. Geophys. Res.-Atmos.*, **106**, 2993–3003, https://doi.org/10.1029/2000JD900652, 2001.

Taylor, K. E., Stouffer, R. J., and Meehl, G. A.: An overview of CMIP5 and the experiment design, *B. Am. Meteorol. Soc.*, **93**, 485–498, https://doi.org/10.1175/BAMS-D-11-00094.1, 2012.

Thomason, L. W. Observations of a new SAGE-II aerosol extinction mode following the eruption of Mt Pinatubo, Geophys. Res. Lett., vol. 19, no. 21, 2179-2182, 1992.

Thomason, L. W., Ernest, N., Millán, L., Rieger, L., Bourassa, A., Vernier, J.-P., Manney, G., Luo, B., Arfeuille, F., and Peter, T.: A global space-based stratospheric aerosol climatology: 1979–2016, Earth Syst. Sci. Data, 10, 469–492, https://doi.org/10.5194/essd-10-469-2018 , 2018.

Thorarinsson, S., Surtsey: island born of fire, *Nat. Geogr. Mag.*, **127**, 5, 713-726, 1965.

Timmreck, C., Mann, G. W., Aquila, V., Hommel, R., Lee, L. A., Schmidt, A., Brühl, C., Carn, S., Chin, M., Dhomse, S. S., Diehl, T., English, J. M., Mills, M. J., Neely, R., Sheng, J., Toohey, M., and Weisenstein, D.: The Interactive Stratospheric Aerosol Model Intercomparison Project (ISA-MIP): motivation and experimental design, *Geosci. Model Dev.*, **11**, 2581–2608, https://doi.org/10.5194/gmd-11-2581-2018, 2018.

~~U. S. Standard Atmosphere, U. S. Gov't. Printing Office, Washington, D. C., 1962.~~

~~Volz, F. E., Photometer mit Selen-Photoelement zur spektralen Messung der Sonnenstrahlung und zur Bestimmung der Wellenlangenabhangigkeit der Dunsttrübung. *Arch. Meteor. Geophys. Bioklim.*, **BIO**, 100-131, 1959~~

~~Volz, F. E., Some results of turbidity networks. *Tellus*, **21**, 625-630, 1969.~~

Volz, F. E., On Dust in the tropical and midlatitude stratosphere from recent twilight measurements, *J. Geophys. Res.* **75**, 1641-1646, 1970.

Went, F. W., Organic matter in the atmosphere, and its possible relation to petroleum formation, *PNAS*, **46** (2) 212-221, https://doi.org/10.1073/pnas.46.2.212 , 1960.

Zanchettin, D., Khodri M., Timmreck C., Toohey M, Schmidt A, Gerber E. P., Hegerl G., Robock A., Pausata F. S. R., Ball W. T., Bauer S. E., Bekki S, Dhomse S. S., LeGrande A. N., Mann, G. W., Marshall L., Mills M., Marchand M., Niemeier U., Poulain V., Rozanov E., Rubino A., Stenke A., Tsigaridis K., Tummon F., The Model Intercomparison Project on the climatic response to volcanic forcing (VolMIP): experimental design and forcing input data for CMIP6. *Geosci. Mod. Dev.*, **9**(8), 2701-2719, https://doi.org/10.5194/gmd-9-2701-2016, 2016.

Con formato: Alemán (Alemania)

Con formato: Hipervínculo, Inglés (Reino Unido)

Con formato: Alemán (Alemania)

Con formato: Color de fuente: Texto 1, Inglés (Reino Unido)

Con formato: Color de fuente: Texto 1

Con formato: Color de fuente: Texto 1, Inglés (Reino Unido)

Con formato: Inglés (Reino Unido)

Con formato: Izquierda, Sangría: Izquierda: 0 cm, Derecha: 0 cm, Interlineado: sencillo, Ajustar espacio entre texto latino y asiático, Ajustar espacio entre texto asiático y números